Variations in nonlocal interaction range lead to emergent chase-and-run in heterogeneous populations

Variations in nonlocal interaction range lead to emergent chase-and-run in heterogeneous populations

K. J. Painter[1], V. Giunta[2], J. R. Potts[3], and S. Bernardi[4]

[1]*Dipartimento Interateneo di Scienze, Progetto e Politiche del Territorio (DIST), Politecnico di Torino, Viale Pier Andrea Mattioli 39, 10125, Turin, Italy*
[2]*Department of Mathematics, Swansea University, Computational Foundry, Bay Campus, Swansea SA1 8EN , UK*
[3]*School of Mathematics and Statistics, Hounsfield Road, University of Sheffield, UK, S3 7RH*
[4]*Department of Mathematical Sciences "G. L. Lagrange", Politecnico di Torino, Corso Duca degli Abruzzi 24, 10129 Torino, Italy*

Abstract

In a chase-and-run dynamic, the interaction between two individuals is such that one moves towards the other (the chaser), while the other moves away (the runner). Examples can be found in both interacting cells and interacting animals. Here we investigate the behaviours that can emerge at a population level, for a heterogeneous group that contains subpopulations of chasers and runners. We show that a wide variety of patterns can form, from stationary patterns to oscillatory and population-level chase-and-run, where the latter describes a synchronised collective movement of the two populations. We investigate the conditions under which different behaviours arise, specifically focusing on the interaction ranges: the distances over which cells or organisms can sense one another's presence. We find that when the interaction range of the chaser is sufficiently larger than that of the runner – or when the interaction range of the chase is sufficiently larger than that of the run – population-level chase-and-run emerges in a robust manner. We discuss the results in the context of phenomena observed in cellular and ecological systems, with particular attention to the dynamics observed experimentally within populations of neural crest and placode cells.

1 Introduction

In cellular and animal systems, interactions frequently trigger movement responses. The collective movements that emerge at a population level have become the focus of considerable interest, in phenomena that range from the swarming and flocking of animals [1], to embryonic development [2], and cancer invasion [3]. Mathematical modelling has helped uncover the mechanistic basis of these emerging dynamics, using methods that range from agent-based (interacting particle systems) to continuous PDE systems [4, 5, 6].

Attraction and repulsion form two fundamental interaction types, whereby the nearby presence of another individual induces movement towards (attraction) or away from it (repulsion). Within a single homogeneous population, attracting interactions can drive a population to self-organise into an aggregated group, such as a herd of animals, while repelling interactions can enhance the dispersal of an aggregated population. For multiple or heterogeneous populations – a mixture of distinct animal species or cell types, or subpopulations with different traits – greater complexity is possible [7]. In a binary system with two distinct populations, there are four principal interactions: a set of two homotypic interactions between individuals of same type, and a set of two heterotypic interactions between individuals of different type. A broad set of interaction combinations can be conjured and the question as to how these subsequently translate into population level dynamics are of manifest interest when it comes to understanding how heterogeneous populations become spatially structured.

Beyond the fundamental nature of an interaction – whether it is attracting or repelling – a second important point of consideration is its range: the distance of separation over which an interaction can occur. These distances will naturally depend on the mechanism through which an interaction

is mediated. Animals and cells can use a multitude of mechanisms to sense other individuals [8], through both direct and indirect means. By direct we mean a sense that could (almost) exactly signal the current position of another individual, for example through directly touching or sighting the neighbour; indirect refers to detection through an intermediary, such as chemical cues or tracks left by the neighbour, that may indicate its recent presence. Whether a sensing is direct or indirect, within heterogeneous groups the interaction ranges of the homotypic and heterotypic interactions could vary considerably: animals range widely with respect to the form and range of their sensory systems – certain species of baleen whales are believed to be possible of communicating over 100s of kilometres [9]; different cells can extend a spectrum of cell protrusions from shorter to long range [10].

We will focus here on a particular type of heterotypic interaction, which we call *chase-and-run* (or pursue-and-escape). Here, individuals of (say) the first population move towards individuals of the second population, which in turn move away. While for the most part we eschew a specific application in favour of broader insights, we note that such dynamics feature within numerous contexts. In an ecological context the obvious example would be between a predator and its prey [11], but it could also occur between dominant and submissive members of a pack. At the cellular level, chase-and-run has been observed both in vitro and in vivo for a variety of heterogeneous cell groups, such as between distinct zebrafish pigment cell types [12] or between embryonic neural crest and placode populations [13].

The case of neural crest and placode cell interactions offers a particularly illuminating exemplar in the context of the objectives here. Chase-and-run in this system is manifested at the population level, demonstrated through in vitro experiments in which a smallish (circa 100 cells) cluster of neural crest cells are cultured close to a similarly-sized cluster of placode cells [13]. These two clusters are subsequently observed to move in concert, maintaining a similar distance of separation as the neural crest cell cluster persistently pursues the cluster of placode cells. Given that certain pathologies may arise from failed migration of neural crest cells to a target tissue [14], the robustness of collective migrations of this nature may be crucial for correct tissue development.

Logically, population-level chase-and-run would seem a natural outcome of chase-and-run interactions at the individual level. However, it would seem equally plausible to suppose other possible outcomes: for example, a running cluster may escape a chasing group and move out of range, or chasers may catch the escaping group. Alternatively, individuals could be chasing one another in a range of different directions, causing the overall populations to be more-or-less homogeneously spread. The objective here is to systematically explore the various dynamics that can emerge within systems where a chase-and-run interaction occurs. To achieve this, in the next section we will describe a somewhat minimal population-level model whereby each interaction is characterised by its *type* (attracting or repelling), *strength*, and *range*. We show that this simple model is capable of exhibiting a broad spectrum of population-level dynamics, including those described above. We subsequently explore the conditions under which particular types of pattern can robustly emerge, focussing on the crucial role played by the interaction ranges.

2 Methods

We present our model as a system of nonlocal advection-diffusion PDEs for continuous population densities, a structure commonly used to phenomenologically describe interaction-based movements in cellular and animal populations (see [6] for a review). However, it is noted that these equations can also be derived through coarse-graining a stochastic individual (agent-based) model, see Supplementary Information (SI); this connection is exploited later to determine the extent to which behaviours observed at the continuous (deterministic) level translate to the discrete (stochastic) level.

The model assumes that movements are governed by a set of homotypic and heterotypic interactions between neighbouring members of two populations: *chasers*, C, and *runners*, R. Neighbouring here refers to those members within a distance specific to a particular interaction. Precisely, we consider (see Figure 1(a)):

- Attracting homotypic interactions. This could represent animal species with naturally tendencies to herd or pack with conspecifics, or cell populations that blue attract each other, e.g. through cell-cell adhesion or ligand-mediated co-attraction.

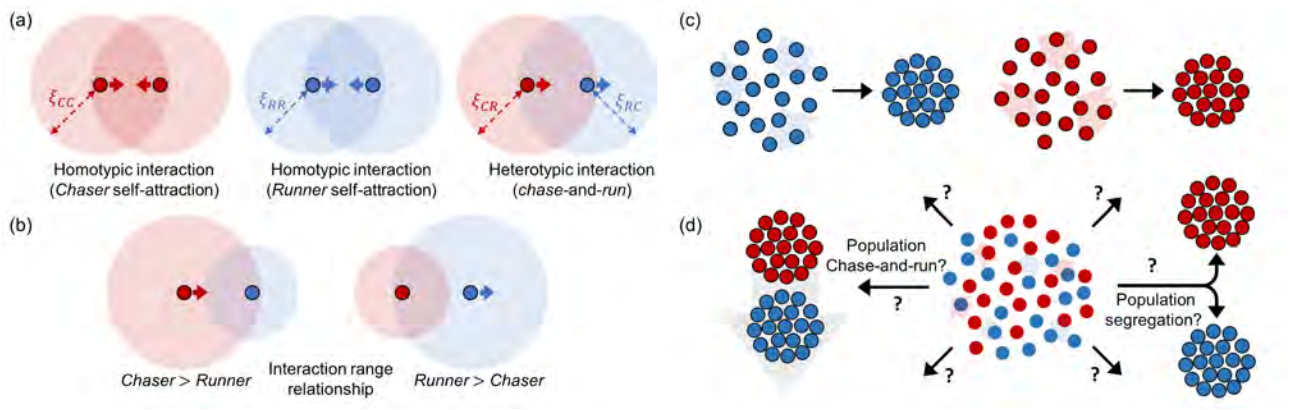

Figure 1: (a) Individual *chasers* (dark red circles) and *runners* (dark blue circles) interact across range ξ_{ij} (light coloured circles) such that (left) chasers are attracted to other chasers, (middle) runners are attracted to other runners, and (right) chase-and-run describes the heterotypic interactions. (b) Distinct ranges lead to various possibilities, such as distances over which (left) chasers detect runners but not vice versa, or (right) runners detect chasers but not vice versa. (c) In the absence of the other population, self-attracting interactions aggregate populations. (d) The principal question we ask in this paper is as follows: in a mixed scenario, what dynamics can arise and what drives the selection of a particular dynamic? Logical reasoning would suggest possibilities that could include a segregated scenario, where the two populations separate into two essentially non-interacting groups, or a population-level chase-and-run dynamic.

- Chase-and-run heterotypic interactions. Specifically, members of C are attracted to neighbouring members of R (the chase), but members of R are repelled by neighbouring members of C (the run).

We note that in real systems a particular interaction could be composed from both attracting and repelling components, e.g. "come close (attraction), but not too close (repulsion)". Incorporating this subtlety would increase parametrisation and complexity, so presently we have reduced to a net interaction: attraction or repulsion. We return to this in the discussion.

Denoting by $C(x,t)$ and $R(x,t)$ the two population densities at position $\mathbf{x} \in \Omega \subset \mathbb{R}^n$ and time $t \in [0,\infty)$, we consider the following system of equations:

$$\frac{\partial C}{\partial t} = \nabla \cdot \left[D_C \nabla C - \frac{C\alpha_{CC}}{V_n(\xi_{CC})}\phi(C+R)\int_{\mathcal{B}^n_{\xi_{CC}}} C(\mathbf{x}+\mathbf{y},t)e_{\mathbf{y}}\,d\mathbf{y} - \frac{C\alpha_{CR}}{V_n(\xi_{CR})}\phi(C+R)\int_{\mathcal{B}^n_{\xi_{CR}}} R(\mathbf{x}+\mathbf{y},t)e_{\mathbf{y}}\,d\mathbf{y}\right], \tag{1a}$$

$$\frac{\partial R}{\partial t} = \nabla \cdot \left[D_R \nabla R - \frac{R\alpha_{RR}}{V_n(\xi_{RR})}\phi(C+R)\int_{\mathcal{B}^n_{\xi_{RR}}} R(\mathbf{x}+\mathbf{y},t)e_{\mathbf{y}}\,d\mathbf{y} - \frac{R\alpha_{RC}}{V_n(\xi_{RC})}\phi(C+R)\int_{\mathcal{B}^n_{\xi_{RC}}} C(\mathbf{x}+\mathbf{y},t)e_{\mathbf{y}}\,d\mathbf{y}\right]. \tag{1b}$$

The three movement terms on the right hand side of (1a) correspond to an undirected (diffusive) component, a directed movement due to homotypic interactions between members of C, and a directed movement due to heterotypic interactions. Correspondingly, those on the right hand side of (1b) derive from diffusive movement, homotypic interactions between members of R, and heterotypic interactions. We use $\mathcal{B}^n_\xi$ to denote the n-dimensional ball of radius ξ, $V_n(\xi)$ to denote its corresponding volume, and set $e_{\mathbf{y}}$ as the unit vector in the direction of $\mathbf{y}$ (if $n = 1$, this is understood to be the sign of y). Models with the above structure have been readily adopted in recent years – see the review [6] and we note in particular a number of studies for two (or more) species for both cellular [15, 16, 17, 18, 19, 20, 21] and ecological [22, 23, 24, 25, 26] interactions.

The direction and strength of each directed movement term is determined according to the integral evaluations of the surrounding population densities, and each requires two parameters, α_{ij} and ξ_{ij}.

Parameters α_{ij}, for $ij \in \{CC, CR, RC, RR\}$, measure the strength and form of response; specifically, the response of members of population i to members of populations j. A positive (negative) value for α_{ij} indicates that i is attracted to (repelled by) j and the magnitude determines the strength of response. Accordingly, to describe our chase-and-run configuration, we concentrate on a regime in which $\alpha_{CC}, \alpha_{RR}, \alpha_{CR} \geq 0$, but $\alpha_{RC} \leq 0$. The parameters ξ_{ij}, for $ij \in \{CC, CR, RC, RR\}$, denote *interaction range* parameters: the maximum separation distance over which each type of interaction can occur. Therefore, a relationship $\xi_{CR} > \xi_{RC}$ implies that the range over which the chase occurs is greater than that of the run (see Figure 1(b)). Note that we will often restrict to a two-dimensional parameter space (ξ_R, ξ_C), where $\xi_{RC} = \xi_{RR} \equiv \xi_R$ represents the runner interaction range and $\xi_{CR} = \xi_{CC} \equiv \xi_C$ represents the chaser interaction range. Restricting to these two parameters could be broadly interpreted as defining distinct perception ranges for each population: ξ_R (or ξ_C) represents the perception range of runners (or chasers), and subsequently defines the maximum range over which its homotypic and heterotypic interactions can form. As a note, for simplicity the model relies on a "top hat" interaction kernel (for other kernels, see [6] and references therein), in which the magnitude of an interaction response does not change with the separation distance (beyond individuals needing to be within the relevant range). The asymmetric interaction (the chase-and-run) coupled to the distinct interaction ranges distinguishes the present work from others noted above, which largely are restricted to symmetric interactions across identical ranges.

We note that D_C and D_R are diffusion coefficients that measure the level of random movement. The function $\phi(C + R)$ curbs directed movement if the population density becomes excessively high. This is not an issue in one dimension, where we will therefore set $\phi(C + R) = 1$ for simplicity. In two dimensions, however, self-attraction tends to generate highly concentrated population densities when $\phi(C + R) = 1$, and we will set $\phi(C + R) = 1/(1 + C + R)$ to avoid this unwanted behaviour in 2D.

We study (1) in both 1D and 2D geometries. To minimise domain/boundary-induced effects we impose wrap-around (periodic) boundary conditions, by setting the domain Ω to be a circle (of circumference L) in 1D, or torus (of dimensions $L \times L$) in 2D. Under these boundary conditions the total population masses are conserved and uniform steady state distributions are therefore determined by the mean initial distributions, i.e. $(C_s, R_s) = \left(\frac{1}{L^n}\int_\Omega C(0,x)dx, \frac{1}{L^n}\int_\Omega R(0,x)dx\right)$. Two forms of initial conditions are considered: *pre-aggregated*, where $C(0,x)$ and $R(0,x)$ are concentrated as Gaussian distributions; *dispersed*, where $C(0,x)$ and $R(0,x)$ are uniform, bar a small random perturbation. For convenience we assume identical diffusion coefficients and mean initial densities and an *a priori* scaling of length, time and densities such that $C_s = R_s = D_C = D_R = 1$.

3 Results

Chase-and-run generates a broad spectrum of population dynamics

To motivate the investigation that follows, we pose a simple question: does chase-and-run at an individual level lead to chase-and-run at the population level? More precisely, can aggregated groups of the two populations move in synchronicity (see Figure 1(d))? Logically, positive homotypic interactions should allow runners and chasers to maintain aggregated forms, and the heterotypic chase-and-run should coordinate the group movements. Simulations confirm this natural conceit, where we observe that two groups placed in proximity (such that a non-negligible level of heterotypic interactions is initially present) form a sustained synchronised movement, see Figure 2(a).

However, this (numerically) stable configuration is found to break down under relatively subtle variations to the interaction strengths. For other parameter combinations we observe population segregation. Here, runners escape the interaction range of chasers and the two populations settle into fixed and separated aggregates, see Figure 2(b), each supported through self-attraction. An alternative form of stationary pattern occurs when chasers are able to reach and trap the runners, resulting in a single mixed aggregate, see Figure 2(c). More complicated dynamics arise for other parameter combinations where, rather than settling into stable chase-and-run or stationary aggregates, we observe sustained oscillations in space and time, which can be both periodic (Figure 2(d)) or aperiodic (Figure 2(e)). Having established that a broad spectrum of patterns are possible, we next explore how interaction range impacts on emergent dynamics in populations of chasers and runners.

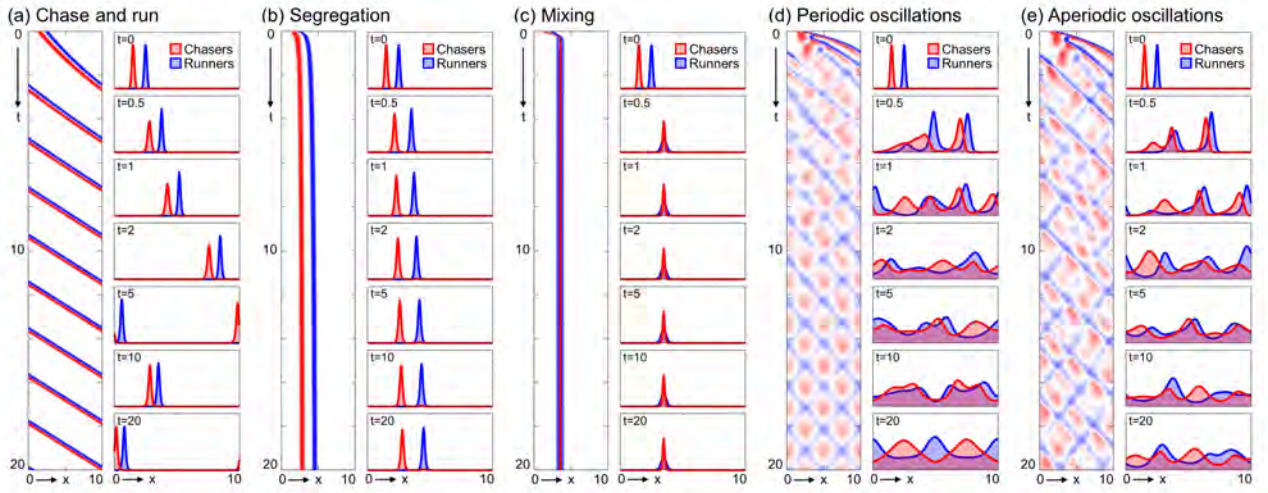

Figure 2: Dynamics of the chase-and-run system (1) in 1D on $[0, 10]$: each panel shows chasers (red) and runners (blue) on a kymograph and distributions at the stated times. Here interaction ranges $\xi_{RR} = \xi_{CR} = \xi_{RC} = \xi_{RR} = 1$ and interactions strengths $\alpha_{CC} = \alpha_{RR} = 3$ with: (a) $(\alpha_{CR}, \alpha_{RC}) = (1, -1)$, (b) $(\alpha_{CR}, \alpha_{RC}) = (2, -3)$, (c) $(\alpha_{CR}, \alpha_{RC}) = (2, -1)$, (d) $(\alpha_{CR}, \alpha_{RC}) = (5, -5)$, (e) $(\alpha_{CR}, \alpha_{RC}) = (4, -4)$. Note that $D_C = D_R = 1$ with initial conditions $C(0, x) = C^* \exp(-50(x - 1.5)^2)$, $R(0, x) = R^* \exp(-50(x - 2.5)^2)$, where C^* and R^* are set such that $C_s = R_s = 1$. For details of the numerical scheme we refer to the SI.

Interaction ranges determine pattern selection

As noted, different interactions may operate across different ranges, e.g. if populations have distinct limits to their perception depth. We consider emergent dynamics across (ξ_R,ξ_C) parameter space from dispersed initial conditions, which allows us to determine whether a particular pattern forms without initial bias. Then, a Turing-type linear stability analysis (LSA) can be used to establish whether the uniform steady state can be unstable to inhomogeneous perturbations and patterns emerge (see SI). Largely speaking, homotypic attractions drive pattern formation – although we note some subtleties that emerge in two dimensions [20] – and allow one or both of the populations to accumulate into one or more groups. The presence of a heterotypic chase-and-run typically leads to a 'Turing-wave' type instability, so that emerging patterns are predicted to oscillate in both space and time; these oscillations are observable in the early time dynamics for each of the simulations plotted in Figure 3(a)ii-v.

LSA provides insight into initial pattern emergence, but for longer time dynamics we rely on numerical simulations. We numerically solve (1) for different (ξ_R,ξ_C) combinations and classify the dynamics at the end of each simulation. We cannot exclude that an observed pattern represents a long-time transient rather than a stable form [27], but simulations are performed for times that extend significantly beyond the characteristic timescale of pattern formation (an order of magnitude or more). Figure 3(a) shows the classification of parameter space, where we observe a clear demarcation into distinct regions. If both species have small interaction ranges, patterns do not form and densities evolve to the uniform steady state solution, Figure 3(a)i – this region coincides with the region of stability predicted by LSA. Intuitively, small interaction ranges limit the size of the observable population and restrict how much interaction-based movement can be generated. Adjacent to this region we observe sustained spatiotemporal oscillations. These transform from periodic and low amplitude (Figure 3(a)ii) to aperiodic and large amplitude (Figure 3(a)iii) with increasing distance from the stability/instability boundary; this coincides with increased pattern growth rates and an increase in the number of unstable modes, predicted by the LSA (see SI).

Setting even larger interaction ranges results in patterns that initially oscillate before transitioning into one of two general forms: a population-level chase-and-run (Figure 3(a)iv) or stationary aggregates (Figure 3(a)v). Significantly, the regions where these two pattern types develop depend on the interaction range relationship. Broadly speaking, population chase-and-run emerges when the chasers

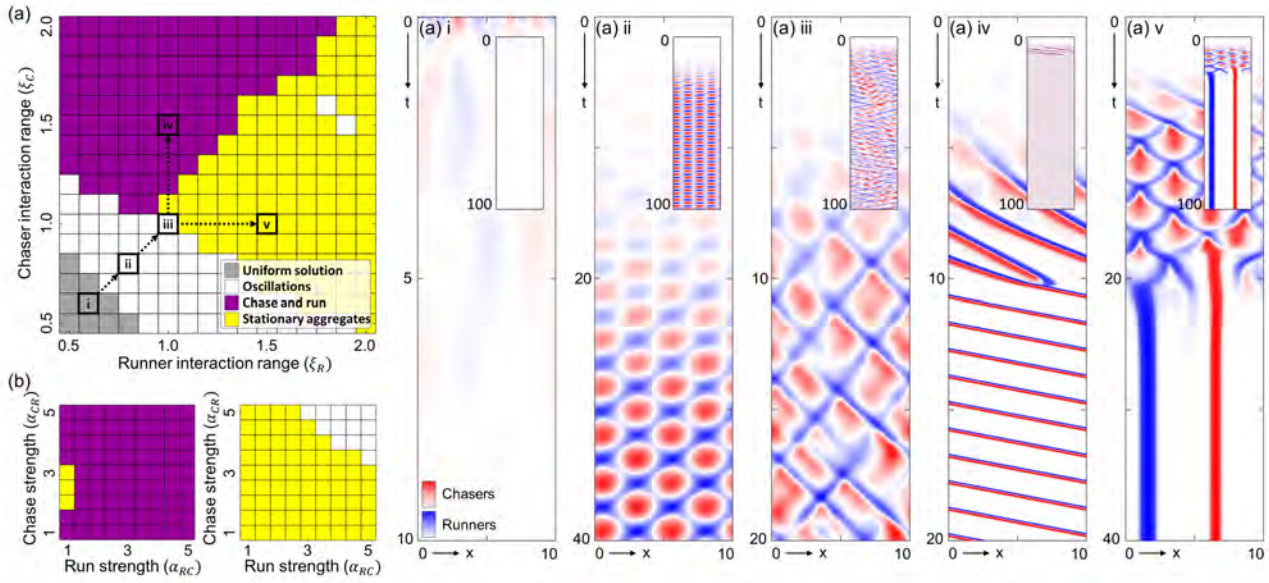

Figure 3: (a) Pattern selection across interaction range space. We classify the pattern for each (ξ_R, ξ_C) pair as: uniform solution (gray), spatiotemporal oscillations (white), population chase-and-run (magenta), stationary aggregates (yellow). The kymographs plotted in (i-v) illustrate representative solutions for certain (ξ_R, ξ_C) pairs, as indicated in (a). For other model parameters, we fix $\alpha_{CC} = \alpha_{CR} = -\alpha_{RC} = \alpha_{RR} = 3$, $D_C = D_R = 1$, $L = 10$ and initial conditions in the dispersed form, such that $C_s = R_s = 1$. (b) Pattern selection across interaction strength space. Here, the pair $(\alpha_{RC}, \alpha_{CR})$ is varied, whilst interaction ranges are selected (left) from the chase and run region (specifically, $(\xi_R, \xi_C) = (1, 1.5)$), and (right) from the stationary aggregates region (specifically, $(\xi_R, \xi_C) = (1.5, 1)$). We fix $D_C = D_R = 1$, $L = 10$ and set initial conditions in the dispersed form. Specifically, we set $C(x, 0) = 1 + r_1(x)$ and $R(x, 0) = 1 + r_2(x)$, where $r_1(x), r_2(x) \in [-0.1, 0.1]$ denote noises added to the uniform steady state densities $(C_s, R_s) = (1, 1)$

have a (sufficiently) larger interaction range than the runners, whereas stationary aggregates form when runners have the larger interaction range. This division is more strongly accentuated when higher interaction strengths are used (see Figure S3(a)), where we find chase-and-run ($\xi_C > \xi_R$) or stationary aggregates ($\xi_C < \xi_R$) and greatly reduced regions of oscillating or uniform solutions. To test whether it is the heterotypic interactions that drive this pattern selection, we see a similar division when only (ξ_{CR}, ξ_{RC}) are varied: $\xi_{CR} > \xi_{RC}$ ($\xi_{RC} > \xi_{CR}$) biases pattern selection to a chase-and-run (stationary) form (Figure S3(b)).

To probe further how the nature of the chase-and-run interactions drive the dynamics, we investigate pattern selection in each of two regimes $\xi_C > \xi_R$ and $\xi_R > \xi_C$, while changing $(\alpha_{RC}, \alpha_{CR})$. This allows a test into the robustness of an observed dynamic while modulating the strength of the heterotypic interactions. Corroborating the key importance of interaction range, we see a robust emergence of chase-and-run across a wide range of interaction strengths, if $\xi_C > \xi_R$ (Figure 3(b), left panel). Similarly, we see robust emergence of stationary aggregates when $\xi_R > \xi_C$ (Figure 3(b), right panel). These explorations also highlight some further subtleties. For example, stationary aggregates are found to range from completely segregated (clusters of only chasers or only runners), to mixed/segregated (some clusters contain both chasers and runners), to completely mixed (the two populations are co-localised), see Figure S3(c). This transition follows changing strengths of the heterotypic interactions: $\alpha_{RC} > \alpha_{CR}$ can allow runners to completely escape chasers and form a separate group, while $\alpha_{CR} > \alpha_{RC}$ can allow chasers to catch and trap runners. Modulations to the chase-and-run can also occur. For example, lower run interaction strength results in some runners being left behind; on the slightly artificial periodic domain, these runners are subsequently recollected and the process repeats (Figure S3(d)).

Summarising, we find that distinct interaction ranges have a strong influence on emergent population level dynamics under chase-and-run type interactions.

Chase-and-run in the plane

In two dimensions a runner can escape a chaser across all angles of the circle. We therefore investigate how dynamics change for populations distributed across $\Omega = [0, L] \times [0, L]$, under the same general homotypic and heterotypic interactions. Populations are initially dispersed (Figure 4(b)) and we again explore (ξ_R, ξ_C)-space. Simulations in this section are accompanied by SI animations.

Principally, we observe the same separation of parameter space into sustained population-level chase-and-run (when $\xi_C > \xi_R$) or stationary aggregates (when $\xi_R > \xi_C$), see Figure 4(a). Consistent with 1D, a more defined separation emerges with higher interaction strengths: lower interaction strengths lead to smaller regions of chase-and-run or stationary aggregates (see Figure S4(a, top)), and larger regions of oscillating (see Figure S4(b)i for an example) or uniform solutions. While chase-and-run is implemented through the heterotypic interactions, increasing the chase-and-run strength alone does not encourage emergence of these dynamics at the population level; in contrast, we see an expansion of the oscillating regime (see Figure S4(a, bottom)). This reinforces that both homotypic and heterotypic interactions play a critical role in setting the population level dynamics.

Consistent with 1D, we find that stationary aggregates range from mixed (Figure 4(c)) to segregated (Figure 4(d)). In regions of chase-and-run, homotypic self-attraction first organises the dispersed populations into clusters. Then, heterotypic interactions drive the cluster of chasers to pursue the cluster of runners, maintaining consistent shape and speed (Figure 4(e), Supplementary Movie 1). This stereotypical chase-and-run robustly emerges when self-interaction strengths are sufficiently strong, and on larger domains (Figure S4(c)). However, some subtler features become apparent according to the runner interaction range. Under more-or-less equal interaction ranges the two groups are roughly equal in size (Figure 4(f), Supplementary Movie 2). Reducing the runner interaction range groups runners into a smaller (and more concentrated) group (Figure 4(e)). Below some critical value, however, runners instead organise into multiple small groups. Run-and-chase still occurs, but in an atypical form: chasers continue to pursue runners, but with multiple runner clusters the chasing direction changes over time (Figure 4(g), Supplementary Movie 3). With its limited interaction range, a cluster of runners remains fixed in position until a chasing group is sufficiently close, at which point it moves away.

To investigate further patterning subtleties, we perturbed specific interaction range parameters

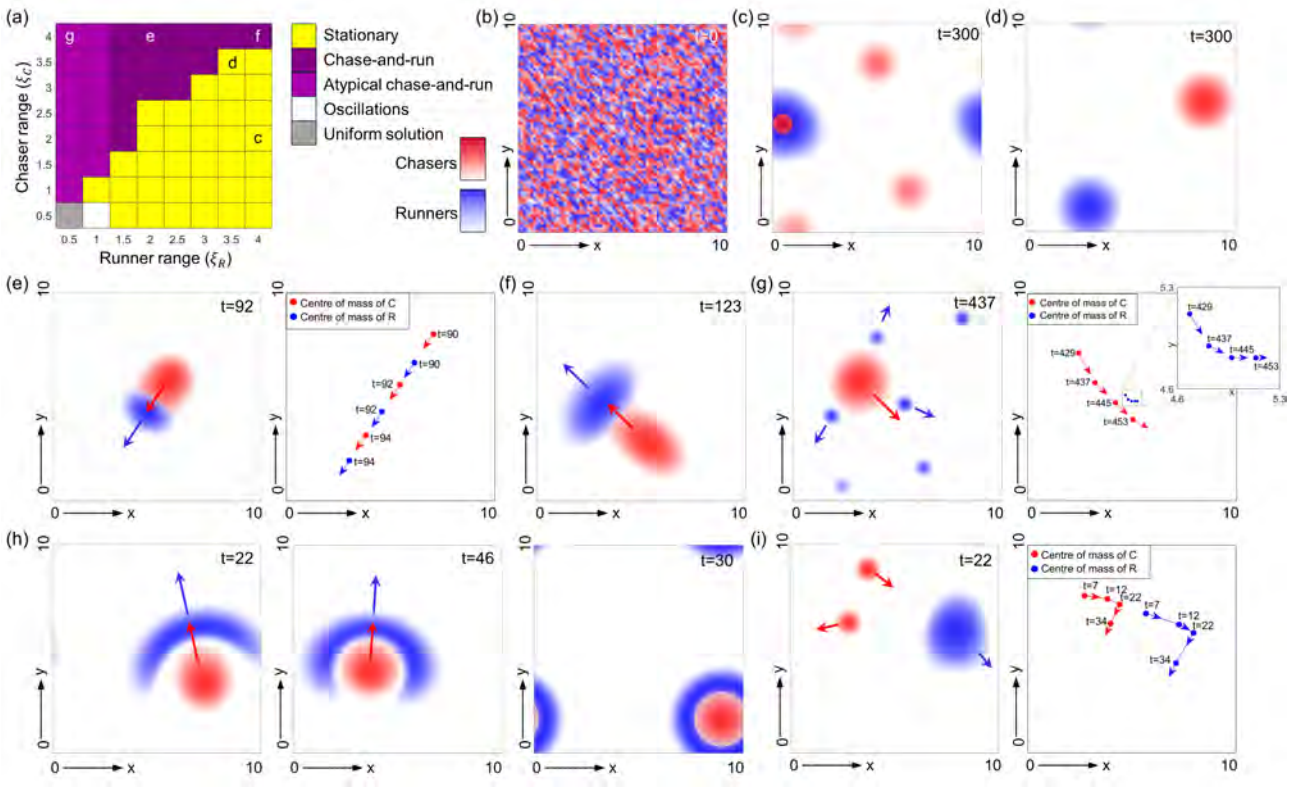

Figure 4: (a) Classification of (ξ_R, ξ_C) parameter space, for simulations of (1) in 2D. (b) Dispersed initial conditions at $t = 0$, specifically $C(x, y, 0) = 1 + r_1(x, y)$ and $R(x, y, 0) = 1 + r_2(x, y)$, where $r_1(x, y), r_2(x, y) \in [-0.1, 0.1]$ denote noises added to the uniform steady state $(C_s, R_s) = (1, 1)$. (c) Stationary aggregate solution found at point **c** in (a). (d) Stationary aggregate solution found at point **d** in (a). (e, left) Stereotypical chase-and-run found at **e** in (a), see Supplementary Movie 1; (e, right panel) The positions of the centre of masses for chasing and running groups over a range of times. (f) Chase-and-run, with interaction ranges found at **f**, see Supplementary Movie 2. (g, left panel) Atypical chase-and-run found at **g** in (a), see Supplementary Movie 3; (g, right panel) Centre of masses for the chasing and the running groups. (h) Crescent-shaped runners for $\xi_{CC} = \xi_{CR} = \xi_{RR} = 4$ and (left) $\xi_{RC} = 2$, (middle) $\xi_{RC} = 1$, (right) $\xi_{RC} = 0.5$. See Supplementary Movies 4-6. (i, left panel) Atypical chase-and-run for $\xi_{CR} = \xi_{RC} = \xi_{RR} = 4$ and $\xi_{CC} = 1$, see Supplementary Movie 7; (i, right panel) Centre of masses for the chasing and the running groups. All simulations in this figure use $\alpha_{CC} = \alpha_{RR} = \alpha_{CR} = -\alpha_{RC} = 15$, $D_C = D_R = 1$, $L_x = L_y = 10$ and $\phi(C + R) = 1/(1 + C + R)$.

and comment on notable instances. Lowering only the run interaction range (ξ_{RC}) leads to a crescent-shaped configuration ahead of the chasing group (Figure 4(h), Supplementary Movies 4-5). Here, runners only detect the nearest portion of the chasing group and, consequently, the escape direction can vary significantly across the runner population. Self-attraction of runners (ξ_{RR}) occurs over longer range, maintaining cohesion and generating the crescent. When ξ_{RC} decreases below a critical value, runners entirely surround chasers in an annulus-like shape, so that net motion is prevented (Figure 4(h), Supplementary Movie 6). Finally, reducing the chaser self-attraction range (ξ_{CC}) below a critical value results in multiple (smaller) chaser groups. At a phenomenological level, the subsequent dynamics can be viewed as a reversal of the atypical chase-and-run above, where now a single group of runners is chased by multiple groups of chasers (Figure 4(i), Supplementary Movie 7). These results highlight that the individual homotypic interaction ranges strongly influence the spatial extension of groups at the population level.

Broadly speaking, investigations in 2D reinforce that interaction ranges dictate the emerging dynamics. Yet we also observe increasingly nuanced patterning, suggesting that greater control is required if a particular pattern is to emerge in higher dimensions.

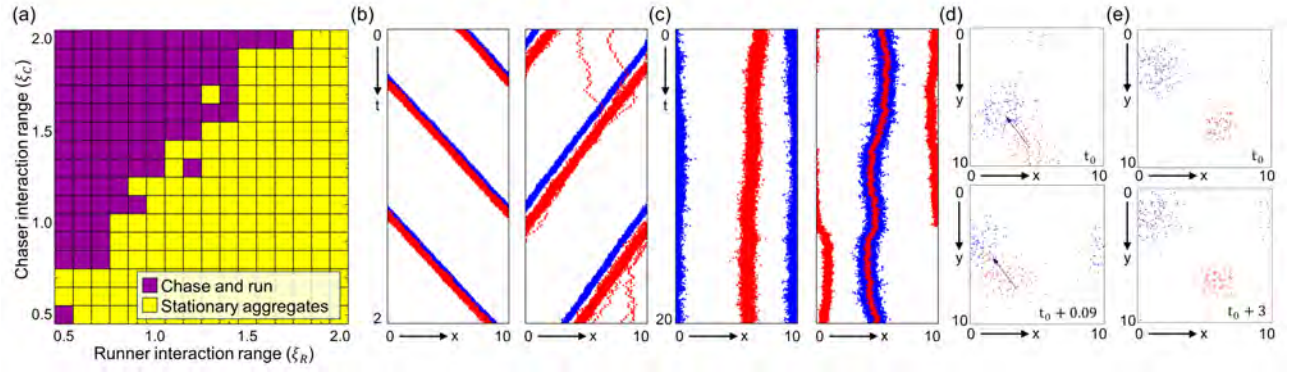

Figure 5: Simulation output of the IBM. (a)-(c) 1D simulations. (a) Classification of (ξ_R, ξ_C) space analogous to Figure 3(a). (b) Representative examples of chase-and-run dynamics in the IBM. (c) Representative examples of stationary aggregate dynamics in the IBM. (d-e) 2D simulations. (d) 2D chase-and-run, analogous to Figure 4(e) with plots showing chasers (red) and runners (blue) at a reference time (top) t_0 and (bottom) $t_0 + 0.09$. (e) 2D stationary aggregates analogous to Figure 4(c) with plots at a reference time (top) t_0 and (bottom) $t_0 + 3$.

Individual-based modelling

The continuous model is predicated on an assumption that the populations can be approximated by density distributions, rather than individual positions. The extent to which this is valid for the population sizes encountered in real-world instances of collective movement is uncertain, and we now determine whether behaviours observed for (1) carry to an individual-based model (IBM). The lattice-based IBM is described in the SI, and features two populations of particles which interact according to the homotypic and heterotypic interactions described previously. Notably, coarse-graining the IBM leads to the continuous formulation given by Equation (1) (see SI). Consequently, an IBM parameter set (including lattice spacing and time step) can be chosen in correspondence to a given simulation of the continuous model. Note that for all IBM simulations we use 100 individuals per populations (consistent with typical sizes of populations of neural crest and placode cells in the example cited in the introduction).

For the 1D IBM (see SI) we consider a lattice of length $L = 10$ with spacing $l = 0.1$. Setting the time step $\tau = 0.005$ then ensures $D = 1$, as used in simulations of the continuous models. As before, we keep $\alpha_{RC} < 0$ and $\alpha_{CC}, \alpha_{CR}, \alpha_{RR} > 0$, so that individuals of population C chase those of population R. In Figure 5(a) we classify the type of pattern observed following simulations of the IBM, covering the same parameter space as in Figure 3(a). Consistent with the continuous model, we see sustained chase-and-run when the interaction range of chasers is large compared to those of the runners (Figure 5(b)), otherwise we see more-or-less stationary aggregates (Figure 5(c)); there can be some 'wobble' in a stationary aggregate position over time, due to inherent stochasticity, but there is no clear chasing. Finer points of detail also translate, such as the range of stationary aggregate patterns from completely segregated to mixed. We further confirmed through simulations of a 2D IBM, using equivalent settings to simulations of the continuous models reported in Figure 4. A population chase-and-run behaviour can be observed when $\xi_C > \xi_R$ (Figure 5 (d)), and stationary aggregates for $\xi_R > \xi_C$ (Figure 5 (e)).

However, some noteworthy differences emerge. First, for the IBM we have not observed (clear) patterns representing homogeneity or sustained oscillations, at least not when using parameter settings equivalent to those within the continuous simulations. This perhaps suggests that these patterns are more reliant on the assumption that a population can be approximated by a continuous distribution, rather than individual positions. Also, in 2D simulations we have found chase-and-runs where the direction of group movements change over time: at lower population sizes, the occasional loss of individuals from runner or chaser groups can prove influential, creating 'rogue' individuals that can subsequently alter cluster dynamics.

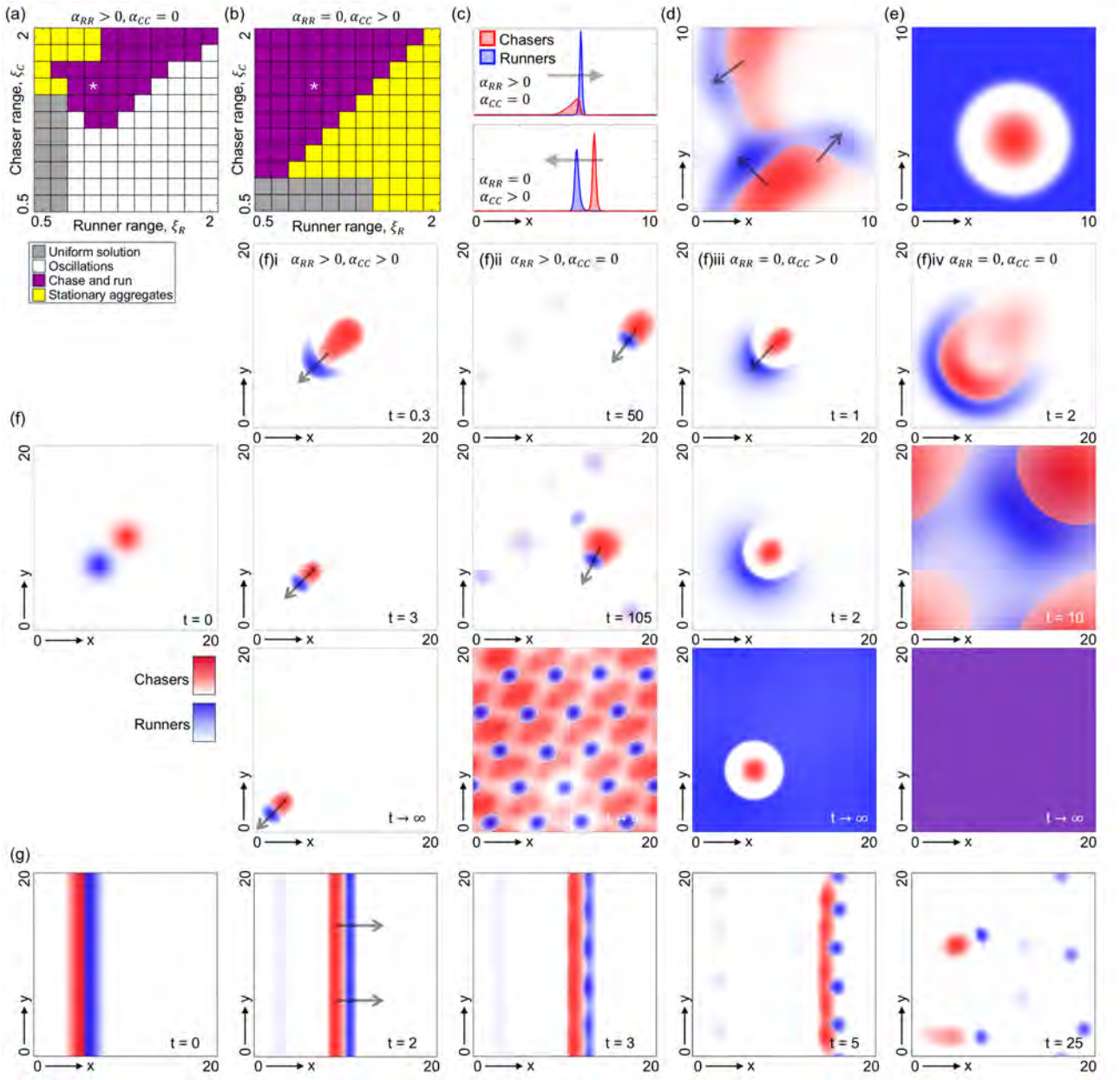

Figure 6: Dynamics for various self-aggregating tendencies. (a-b) Classification of (ξ_R, ξ_C)-space for (1) in 1D with $\alpha_{CR} = 3, \alpha_{RC} = -3$ and $(\alpha_{RR}, \alpha_{CC}) =$ (a) $(3, 0)$, (b) $(0, 3)$. (c) Typical chase-and-run profiles in 1D, for positions marked with the white star in (a-b). (d) Irregular chase-and-run in 2D when only runners self-aggregate, from dispersed initial conditions (Supplementary Movie 8). Here, $\xi_C = 4, \xi_R = 3, \alpha_{RR} = \alpha_{CR} = 15, \alpha_{RC} = -15, \alpha_{CC} = 0$. (e) Stationary aggregate of chasers in 2D when only chasers self-aggregate. Here, $\xi_C = 4, \xi_R = 2, \alpha_{CC} = \alpha_{CR} = 15, \alpha_{RC} = -15, \alpha_{RR} = 0$. (f) Pre-aggregated initial conditions $C(x, y, 0) = C^* \exp\left(-0.2(x-10)^2 - 0.2(y-10)^2\right)$, $R(x, y, 0) = R^* \exp\left(-0.2(x-7)^2 - 0.2(y-7)^2\right)$, where C^* and R^* are such that $C_s = R_s = 1$ (left panel). Columns from left to right show snapshots for $(\alpha_{CC}, \alpha_{RR}) =$ (i) $(15, 15)$, (ii) $(0, 15)$ (Supplementary Movie 9), (iii) $(15, 0)$ (Supplementary Movie 10), (iv) $(0, 0)$. Other parameters set at $\xi_C = 4, \xi_R = 2, \alpha_{CR} = 15, \alpha_{RC} = -15$ and "$t \to \infty$" indicates the long time pattern form. (g) Populations initially arranged into parallel stripes, specifically a small random perturbation of $C(x, y, 0) = C^* \exp\left(-(x-5)^2\right)$, $R(x, y, 0) = R^* \exp\left(-(x-6)^2\right)$, where C^* and R^* are such that $C_s = R_s = 1$. Other parameter values are $\alpha_{CC} = \alpha_{CR} = -\alpha_{RC} = \alpha_{RR} = 15, \xi_C = 4, \xi_R = 2$. All simulations use $D_C = D_R = C_s = R_s = 1$.

Self-attraction is required for robust chase-and-run

We have observed how population chase-and-run emerges in 1D, 2D and in IBM simulations, when the range of the chase is greater than that of the run. However, all simulations to date assume that

each population has a self-attraction that allow their self-aggregation. We investigate whether this is crucial for the emergence and maintenance of a pattern type.

First we repeat the 1D analysis, investigating pattern selection in (ξ_R, ξ_C)-space under two cases: (i) only runners self-aggregate ($\alpha_{RR} > 0$, $\alpha_{CC} = 0$); (ii) only chasers self-aggregate ($\alpha_{CC} > 0$, $\alpha_{RR} = 0$). In both instances we (broadly) find the same behaviour: across a large region of parameter space corresponding to $\xi_C > \xi_R$, a sustained chase-and-run emerges at the population scale (Figure 6(a-b)). Self-aggregation in the runners leads to their clustering which – via the heterotypic interactions – collect chasers into a looser group in the rear (Figure 6(c), top). Self-aggregation in the chasers lead to a chaser cluster that 'herds' runners ahead (Figure 6(c), bottom).

However, these observations of emergent and sustained chase-and-run in 1D evaporate in higher dimensions. When only runners aggregate, scenarios of chase-and-run ($\xi_C > \xi_R$) become 'incoherent', with the groups repeatedly splitting and reforming over time (Figure 6(d), see supplementary Movie 8). Here, the somewhat dispersed chasing group transmits variable directional information into the cluster of runners, inducing their escape into directions that can split the group; the reformation of groups can be part-attributed to the peculiarities of the boundary conditions. When only chasers aggregate, a $\xi_C > \xi_R$ scenario leads to a stationary cluster of chasers surrounded by uniformly dispersed runners (Figure 6(e)). Unlike in 1D, where runners can be herded and trapped by the geometry, different escape directions mean that runners spread until chasers have no coherent direction of pursuit.

To test this under a more controlled setting, chasers and runners are initialised as juxtaposed clusters, Figure 6(f): this could be regarded as an optimal initial state to encourage chase-and-run. Also, to limit the influence of boundary conditions we consider a larger domain. Setting $\xi_C > \xi_R$, if both populations self-aggregate we observe robust and coherent chase-and-run in (seeming) perpetuity (Figure 6(f)i). When only runners self-aggregate a transient chase-and-run can occur, but the runner and chaser groups lose mass over time and eventually chase-and-run disintegrates (Figure 6(f)ii, see Supplementary Movie 9). When only chasers self-aggregate, any chase-and-run is extremely brief: the runners quickly disperse in all directions to leave a stranded group of chasers (Figure 6(f)iii, see Supplementary Movie 10). Similarly, when neither population can self-aggregate any coherent motion is transient and the populations disperse to the uniform steady state (Figure 6(f)iv). Finally, we investigate dynamics for populations that are initially arranged into stripes (Figure 6(g)), for the same interactions as in Figure 6(f)i. At first the populations move in stripes of chasers and runners, before the front destabilises and resolves into discrete clusters that undergo separate chase-and-run. This clustering principally stems from the self-attraction terms that round populations into compact groups.

4 Discussion

We have explored the collective dynamics that emerge within mixed populations of chasers and runners, where the two populations have an inherent tendency to aggregate with members of their own kind and pursue and evade the other population, respectively. Focussing on the interaction ranges, we observe two dominating pattern forms: (i) when runners interact over larger distances than chasers (or the range of the run is greater than that of the chase), quasi-stationary and separated clusters emerge that undergo negligible interaction; (ii) when chasers interact over larger distances than runners (or the range of the chase is greater than that of the run), a collective chase-and-run forms where the cluster of chasers pursues the cluster of runners. Given sufficiently strong interaction strengths, this overall observation is apparently robust with respect to moderate parameter variations, when extended into a higher dimension setting, and when examined within the finite population sizes and stochastic setting of a corresponding individual-based model. As such, distinct interaction ranges between species appear to significantly determine emergent collective dynamics.

Intentionally, we have formulated the model in a minimal and generic manner, so that (in principal) the results could be interpreted for cellular or animal populations. For the former, chase-and-run dynamics have been observed in zebrafish pigment cells [12] and *Xenopus laevis* neural crest cell (NCC)–placode cell (PC) populations [13]. The latter forms a particularly apposite example, as *in vitro* studies reveal an analogous phenomenon of population-level chase-and-run [13]: NCCs form the chasing group, and PCs the running group. Experiments have uncovered various cellular interactions, including

contact inhibition of locomotion (CIL) [28, 13] between all cells: the touching of two cells reverses their movement directions. Consequently, CIL forms a repulsion between all cells, but other interactions may switch some of these to attracting. First, PCs adhere to each other (through E-cadherin), which overcomes CIL to allow PC-to-PC attraction [13]. Second, attracting homotypic interactions also occur between NCCs [29, 30], seemingly autotaxis-mediated through a secreted attractant. Third, NCCs are attracted to PCs through the latter secreting a chemotaxis factor (Sdf-1) [13]. Under the reductive reasoning of a considered 'net interaction', it is plausible that the set of interactions may conform to those explored here and we predict that a robust population chase-and-run will arise if NCCs interact over larger ranges. Indeed, this is quite plausible: PC interactions are seemingly through direct contact (membrane-membrane binding), while NCC interactions involve diffusing ligands. The simulations presented in Figure 6(f) are particularly apposite for this application, as the *in vitro* experiments place NCCs and PCs as juxtaposed clusters (akin to the $t = 0$ setting of those simulations). While indefinite chase-and-run requires both populations to have self-attraction, long transient chase-and-runs can still occur when only the runners have (strong) self-attraction: if this transient is much longer than the timescale of experiments, this may be sufficient. Thus, our simulations would suggest that while strong self-attraction is essential in the runner group (i.e. the PCs), a similar requirement may not be strictly necessary for the chasers (i.e. the NCs); possibly this could be tested through knocking out the mechanism of co-attraction between NC cells.

Initialising as clusters recapitulates an *in vitro* setting. The neural crest itself forms along the dorsal neural tube, creating a 'stripe' along the vertebrate embryo. Experimental observations of the *Xenopus* NCC-PC system – and simulations of an ABM – have revealed that as the NCCs move away from the crest, they insert into alternating 'streams' with the surrounding PCs [31]. In other words, a form of symmetry-breaking takes place along the length of the (cranial) neural crest. Our simulations with a stripe setting (Figure 6(g)) also show a symmetry-breaking, with the stripe destabilising into multiple clusters. We do not, however, observe a formation of alternating streams. This is not in itself surprising, given that our (current) model is not explicitly tailored to describe this particular application. A more considered investigation would be a very interesting avenue, necessitating extension to a 'next level' model, for example: dropping the reduction to a net interaction, so that the relationship between two cell types may be composed from both repulsive (e.g. CIL) and attractive (e.g. co-attraction) interactions; explicitly modelling key extracellular factors (e.g. Sdf-1), receptor-ligand interactions etc; parametrising the model as far as possible according to data. This would offer a complementary approach for modelling the *Xenopus* NCC-PC system, as previous approaches have been restricted to agent-based models (e.g. [31, 32]).

In ecology, our chase-and-run can be viewed analogously to a pursuit and escape interaction and the model described here could help in understanding the spatial arrangements of predators and prey on a landscape. The concept of a 'landscape of fear', whereby prey avoid areas they believe predators to be living, has gained much attention in recent years [33, 34]. Improvements in animal tracking technology [35] have begun to allow researchers to map such landscapes and rigorously demonstrate prey avoidance [36, 37]. Likewise, the notion of prey-taxis [38], whereby predators seek to locate themselves near prey, is well-understood from both empirical [39] and mathematical [40] perspectives. Both aspects have been studied mathematically in a model similar to ours but with quadratic rather than linear diffusion [41]. However, in empirical situations, it is less clear whether a combination of predator-avoidance and prey-taxis behaviour ever actually leads to the kind of population-level chase-and-run described here. Indeed, empirical evidence suggests that most animals tend to locate themselves in relatively-stationary home ranges rather than moving over the landscape in response to predation pressure or seeking out mobile prey [42]. A possible reason for this is that landscape heterogeneity might 'pin' the population-level movements, so that, for example, prey might spend time in a woodland area where they can hide from predators, whereas predators might live close to the forest in hope of catching any prey that venture out [43]. Mathematical investigation of individual-level chase-and-run within heterogeneous environments would help understand why we still tend to see predators and prey using relatively stationary home ranges, despite the theoretical possibility of population-level chase-and-run in homogeneous environments.

Notions of followers and leaders have gathered considerable traction in recent years [44, 45, 46, 47, 3]. The terms 'followers' and 'leaders' imply a hierarchy – the latter guide the former – though in some cases their designations may simply reflect a spatial position [48]: leaders at the front, followers

at the rear. Placed in the context of the collective run-and-chase that emerges here, the macroscopic perspective is runners at the front and chasers at the rear. But regarding runners as leaders and chasers as followers is clearly misleading: while the groups sort into a structured arrangement, there is no overall guidance and the net movement (from unbiased initial conditions) will be at random. This susceptibility is highlighted by the (2D) IBM simulations, where the chase-and-run direction was deflected by 'rogue' individuals and/or stochastic fluctuations. The addition of a further directional bias – such as a chemoattractant – could confer a robustness to the global direction of movement and in this regard it may be illuminating to observe how robustness alters according to which population detects the global cue: under what circumstances do runners or chasers make the more effective leaders?

Coherent chase-and-run – by which we mean a compact cluster of chasers pursuing a compact cluster of runners – was found to emerge in both 1D and 2D. In 1D this is particularly robust, given the stipulated relationship between interaction ranges, within both continuous and IBM formulations. Of course, this robustness can be partly attributed to the peculiarities of a 1D geometry, where runners can only escape in one of two possible directions. Away from singular or engineered instances – such as cells restricted to lines along microfabricated surfaces [49] – movements take place in higher dimensions, e.g. two dimensions for cells plated on a surface or animal movements on the plane. Despite the greater freedom movement direction, coherent chase-and-run does emerge robustly in two dimensions, but with caveats: for example (in continuous simulations) 'complex' chase-and-runs where the dynamics of a single large cluster of runners (chasers) is driven by multiple smaller groups of chasers (runners), or (in IBM simulations) with occasional fluctuations in the movement direction. Emergence of a particular dynamic in two dimensions may therefore require additional 'control', e.g. more tightly controlled parameters or reinforcement through environmental heterogeneity. A number of modelling and experimental studies have suggested that microenvironmental factors may indeed play an important role in confining collective migration of neural crest cells along particular pathways [50, 51].

We have observed even more diverse pattern forms in certain regimes, including a menagerie of oscillatory dynamics. These dynamics were robust – in the sense that they continued indefinitely and persisted under perturbation – and therefore seemingly represent a stable pattern outcome of the continuous model, rather than a transient dynamic. A deeper analytical study into the patterns that arise as parameters are varied could be achieved through nonlinear bifurcation analyses [52], a possible future direction. However, is is noted that in the IBM these oscillatory dynamics were conspicuous by their absence: under equivalent parameters, solutions evolved to either the population chase-and-run or stationary aggregate patterns. The continuous model assumes that populations can be approximated by a continuous density rather than individual particle positions, and it is possible that simulations of the IBM under larger populations would reveal similar phenomena. It should also be noted that an IBM will introduce other forms of artificiality – for example, the IBM here is based on point-particles that make instantaneous jumps in individual location – which could generate particularly high levels of stochasticity. Convergence to the continuous model involves various limits (e.g. smaller steps, higher population sizes), and a more detailed investigation into the correspondence between the IBM and continuous model may pinpoint scenarios under which particular outcomes may be expected to arise. It may also be worth investigating whether different IBM frameworks – for example, those where particles move continuously through space – can be scaled to the same continuous model, and whether those lead to different behaviours. Overall, though, the discrepancies we have observed reinforce a general lesson that caution should be adopted regarding 'exotic' patterning phenomena observed in models, particularly when found in restricted regions of parameter space.

A number of earlier studies have used similar modelling frameworks to understand the distinct patterns that can arise from self and cross interactions within heterogeneous systems. Several of these have been motivated by adhesive cell sorting, for example see [15, 53, 17, 18, 19, 21, 20]. Here, homotypic and heterotypic interactions are typically nonnegative and studies have focussed on how distinct adhesions lead to distinct arrangements, consistent with classical predictions of the differential adhesion hypothesis [54]. A generalisation to interactions that range from attracting to repelling was conducted in [16], although the subsequent analysis was primarily restricted to simple one-dimensional geometries and equivalent interaction ranges. Recently, Jewell et al [20] have extended this to two dimensions where, surprisingly, a pure chase-and-run interaction (with no homotypic interactions) was

shown to be capable of generating pattern formation in two (and higher) dimensions. Significantly, unequal interaction ranges form a requirement and the study here further reinforces the critical role that interaction ranges can play in patterning dynamics.

We have shown that wide-ranging collective dynamics can emerge, even for just two species undergoing chase-and-run interactions. Yet, the relatively simple assumption of distinct interaction ranges provides a powerful point of control, strongly determining pattern selection. Clearer understanding into the ranges over which particular interactions are mediated would provide valuable information into the organisation of complex systems.

Ethics. This work did not require ethical approval from a human subject or animal welfare committee.
Competing Interests. We declare we have no competing interests.
Data Access. Code available at `https://zenodo.org/records/13772853`.
Author Contributions. SB - formal analysis, investigation, methodology, writing-reviewing and editing; VG - formal analysis, investigation, methodology, writing-reviewing & editing; KJP - conceptualisation, formal analysis, investigation, methodology, writing-original draft, writing-reviewing & editing; JRP - formal analysis, investigation, methodology, writing-reviewing and editing
Funding. KJP acknowledges 'Miur-Dipartimento di Eccellenza' funding to the Dipartimento di Scienze, Progetto e Politiche del Territorio (DIST). JRP and VG acknowledge support of Engineering and Physical Sciences Research Council (EPSRC) grant EP/V002988/1 awarded to JRP. SB and VG acknowledge the financial support of GNFM-INdAM through 'INdAM – GNFM Project', CUP E53C22001930001.
Acknowledgements. We thank Alf Gerisch and Nadir Fasola for assistance and advice regarding numerical implementation. KJP and SB are members of INdAM-GNFM.

References

[1] DJ Sumpter. *Collective animal behavior*. Princeton University Press, 2010.

[2] E Scarpa and R Mayor. "Collective cell migration in development". In: *Journal of Cell Biology* 212.2 (2016), pp. 143–155.

[3] SA Vilchez Mercedes, F Bocci, H Levine, JN Onuchic, MK Jolly, and PK Wong. "Decoding leader cells in collective cancer invasion". In: *Nature Reviews Cancer* 21.9 (2021), pp. 592–604.

[4] S Motsch and E Tadmor. "Heterophilious dynamics enhances consensus". In: *SIAM Review* 56.4 (2014), pp. 577–621.

[5] AM Berdahl, AB Kao, A Flack, PA Westley, EA Codling, ID Couzin, AI Dell, and D Biro. "Collective animal navigation and migratory culture: from theoretical models to empirical evidence". In: *Philosophical Transactions of the Royal Society B: Biological Sciences* 373.1746 (2018), p. 20170009.

[6] KJ Painter, T Hillen, and JR Potts. "Biological modelling with nonlocal advection diffusion equations". In: *Mathematical Models and Methods in Applied Sciences (M3AS)* 34 (2023), pp. 57–107.

[7] JR Potts and MA Lewis. "Spatial memory and taxis-driven pattern formation in model ecosystems". In: *Bulletin of Mathematical Biology* 81 (2019), pp. 2725–2747.

[8] CUM Smith. *Biology of sensory systems*. John Wiley & Sons, 2008.

[9] R Payne and D Webb. "Orientation by means of long range acoustic signaling in baleen whales". In: *Annals of the New York Academy of Sciences* 188.1 (1971), pp. 110–141.

[10] YM Yamashita, M Inaba, and M Buszczak. "Specialized intercellular communications via cytonemes and nanotubes". In: *Annual Review of Cell and Developmental Biology* 34 (2018), pp. 59–84.

[11] TY Moore and AA Biewener. “Outrun or outmaneuver: predator–prey interactions as a model system for integrating biomechanical studies in a broader ecological and evolutionary context”. In: *Integrative and Comparative Biology* 55.6 (2015), pp. 1188–1197.

[12] H Yamanaka and S Kondo. “In vitro analysis suggests that difference in cell movement during direct interaction can generate various pigment patterns in vivo”. In: *Proceedings of the National Academy of Sciences* 111.5 (2014), pp. 1867–1872.

[13] E Theveneau, B Steventon, E Scarpa, S Garcia, X Trepat, A Streit, and R Mayor. “Chase-and-run between adjacent cell populations promotes directional collective migration”. In: *Nature Cell Biology* 15.7 (2013), pp. 763–772.

[14] GA Vega-Lopez, S Cerrizuela, C Tribulo, and MJ Aybar. “Neurocristopathies: New insights 150 years after the neural crest discovery”. In: *Developmental Biology* 444 (2018), S110–S143.

[15] NJ Armstrong, KJ Painter, and JA Sherratt. “A continuum approach to modelling cell–cell adhesion”. In: *Journal of Theoretical Biology* 243.1 (2006), pp. 98–113.

[16] KJ Painter, J Bloomfield, J Sherratt, and A Gerisch. “A nonlocal model for contact attraction and repulsion in heterogeneous cell populations”. In: *Bulletin of Mathematical Biology* 77 (2015), pp. 1132–1165.

[17] H Murakawa and H Togashi. “Continuous models for cell–cell adhesion”. In: *Journal of Theoretical Biology* 374 (2015), pp. 1–12.

[18] JA Carrillo, Y Huang, and M Schmidtchen. “Zoology of a nonlocal cross-diffusion model for two species”. In: *SIAM Journal on Applied Mathematics* 78.2 (2018), pp. 1078–1104.

[19] JA Carrillo, H Murakawa, M Sato, H Togashi, and O Trush. “A population dynamics model of cell-cell adhesion incorporating population pressure and density saturation”. In: *Journal of Theoretical Biology* 474 (2019), pp. 14–24.

[20] TJ Jewell, AL Krause, PK Maini, and EA Gaffney. “Patterning of nonlocal transport models in biology: the impact of spatial dimension”. In: *Mathematical Biosciences* 366 (2023), p. 109093.

[21] C Falcó, RE Baker, and JA Carrillo. “A local continuum model of cell-cell adhesion”. In: *SIAM Journal on Applied Mathematics* (2023), S17–S42.

[22] P Amorim, B Telch, and LM Villada. “A reaction–diffusion predator–prey model with pursuit, evasion, and nonlocal sensing”. In: *Mathematical Biosciences and Engineering* 16.5 (2019), pp. 5114–5145.

[23] E Ellefsen and N Rodriguez. “On equilibrium solutions to nonlocal mechanistic models in ecology”. In: *Journal of Applied Analysis and Computation* 11.6 (2021).

[24] V Giunta, T Hillen, M Lewis, and JR Potts. “Local and global existence for nonlocal multispecies advection-diffusion models”. In: *SIAM Journal on Applied Dynamical Systems* 21.3 (2022), pp. 1686–1708.

[25] V Giunta, T Hillen, MA Lewis, and JR Potts. “Detecting minimum energy states and multistability in nonlocal advection–diffusion models for interacting species”. In: *Journal of Mathematical Biology* 85.5 (2022), p. 56.

[26] H Wang and Y Salmaniw. “Open problems in PDE models for knowledge-based animal movement via nonlocal perception and cognitive mapping”. In: *Journal of Mathematical Biology* 86.5 (2023), p. 71.

[27] JR Potts and KJ Painter. “Distinguishing between long-transient and asymptotic states in a biological aggregation model”. In: *Bulletin of Mathematical Biology* 86.3 (2024), pp. 1–16.

[28] C Carmona-Fontaine, HK Matthews, S Kuriyama, M Moreno, GA Dunn, M Parsons, CD Stern, and R Mayor. “Contact inhibition of locomotion in vivo controls neural crest directional migration”. In: *Nature* 456.7224 (2008), pp. 957–961.

[29] E Theveneau, L Marchant, S Kuriyama, M Gull, B Moepps, M Parsons, and R Mayor. “Collective chemotaxis requires contact-dependent cell polarity”. In: *Developmental Cell* 19.1 (2010), pp. 39–53.

[30] C Carmona-Fontaine, E Theveneau, A Tzekou, M Tada, M Woods, KM Page, M Parsons, JD Lambris, and R Mayor. "Complement fragment C3a controls mutual cell attraction during collective cell migration". In: *Developmental Cell* 21.6 (2011), pp. 1026–1037.

[31] A Szabó, E Theveneau, M Turan, and R Mayor. "Neural crest streaming as an emergent property of tissue interactions during morphogenesis". In: *PLoS computational biology* 15.4 (2019), e1007002.

[32] A Colombi, M Scianna, KJ Painter, and L Preziosi. "Modelling chase-and-run migration in heterogeneous populations". In: *Journal of Mathematical Biology* 80.1 (2020), pp. 423–456.

[33] JW Laundré, L Hernández, and WJ Ripple. "The landscape of fear: ecological implications of being afraid". In: *The Open Ecology Journal* 3.1 (2010).

[34] KM Gaynor, JS Brown, AD Middleton, ME Power, and JS Brashares. "Landscapes of fear: spatial patterns of risk perception and response". In: *Trends in Ecology & Evolution* 34.4 (2019), pp. 355–368.

[35] HJ Williams, LA Taylor, S Benhamou, AI Bijleveld, TA Clay, S de Grissac, U Demšar, HM English, N Franconi, A Gómez-Laich, et al. "Optimizing the use of biologgers for movement ecology research". In: *Journal of Animal Ecology* 89.1 (2020), pp. 186–206.

[36] G Bastille-Rousseau, JR Potts, JA Schaefer, MA Lewis, EH Ellington, ND Rayl, SP Mahoney, and DL Murray. "Unveiling trade-offs in resource selection of migratory caribou using a mechanistic movement model of availability". In: *Ecography* 38.10 (2015), pp. 1049–1059.

[37] TR Ganz, MT DeVivo, AJ Wirsing, SB Bassing, BN Kertson, SL Walker, and LR Prugh. "Cougars, wolves, and humans drive a dynamic landscape of fear for elk". In: *Ecology* (2024), e4255.

[38] P Kareiva and G Odell. "Swarms of predators exhibit "preytaxis" if individual predators use area-restricted search". In: *The American Naturalist* 130.2 (1987), pp. 233–270.

[39] AC Nisi, JP Suraci, N Ranc, LG Frank, A Oriol-Cotterill, S Ekwanga, TM Williams, and CC Wilmers. "Temporal scale of habitat selection for large carnivores: Balancing energetics, risk and finding prey". In: *Journal of Animal Ecology* 91.1 (2022), pp. 182–195.

[40] JM Lee, T Hillen, and MA Lewis. "Pattern formation in prey-taxis systems". In: *Journal of Biological Dynamics* 3.6 (2009), pp. 551–573.

[41] S Fagioli and Y Jaafra. "Multiple patterns formation for an aggregation/diffusion predator-prey system". In: *Networks and Heterogeneous Media* 16.3 (2021), pp. 377–411.

[42] L Börger, BD Dalziel, and JM Fryxell. "Are there general mechanisms of animal home range behaviour? A review and prospects for future research". In: *Ecology Letters* 11.6 (2008), pp. 637–650.

[43] N Bonnot, N Morellet, H Verheyden, B Cargnelutti, B Lourtet, F Klein, and AM Hewison. "Habitat use under predation risk: hunting, roads and human dwellings influence the spatial behaviour of roe deer". In: *European Journal of Wildlife Research* 59 (2013), pp. 185–193.

[44] J Krause, D Hoare, S Krause, C Hemelrijk, and D Rubenstein. "Leadership in fish shoals". In: *Fish and Fisheries* 1.1 (2000), pp. 82–89.

[45] SA Rands, G Cowlishaw, RA Pettifor, JM Rowcliffe, and RA Johnstone. "Spontaneous emergence of leaders and followers in foraging pairs". In: *Nature* 423.6938 (2003), pp. 432–434.

[46] R McLennan, LJ Schumacher, JA Morrison, JM Teddy, DA Ridenour, AC Box, CL Semerad, H Li, W McDowell, D Kay, et al. "Neural crest migration is driven by a few trailblazer cells with a unique molecular signature narrowly confined to the invasive front". In: *Development* 142.11 (2015), pp. 2014–2025.

[47] S Nakayama, JL Harcourt, RA Johnstone, and A Manica. "Who directs group movement? Leader effort versus follower preference in stickleback fish of different personality". In: *Biology Letters* 12.5 (2016), p. 20160207.

[48] E Theveneau and C Linker. “Leaders in collective migration: are front cells really endowed with a particular set of skills?” In: *F1000Research* 6 (2017).

[49] E Scarpa, A Roycroft, E Theveneau, E Terriac, M Piel, and R Mayor. “A novel method to study contact inhibition of locomotion using micropatterned substrates”. In: *Biology Open* 2.9 (2013), pp. 901–906.

[50] A Szabó, M Melchionda, G Nastasi, ML Woods, S Campo, R Perris, and R Mayor. “In vivo confinement promotes collective migration of neural crest cells”. In: *Journal of Cell Biology* 213.5 (2016), pp. 543–555.

[51] R McLennan, R Giniunaite, K Hildebrand, JM Teddy, JC Kasemeier-Kulesa, L Bolanos, RE Baker, PK Maini, and PM Kulesa. “Colec12 and Trail signaling confine cranial neural crest cell trajectories and promote collective cell migration”. In: *Developmental Dynamics* 252.5 (2023), pp. 629–646.

[52] V Giunta, T Hillen, MA Lewis, and JR Potts. “Weakly nonlinear analysis of a two-species non-local advection–diffusion system”. In: *Nonlinear Analysis: Real World Applications* 78 (2024), p. 104086.

[53] A Gerisch and KJ Painter. “Mathematical modelling of cell adhesion and its applications to developmental biology and cancer invasion”. In: vol. 2. CRC Press Boca Raton, 2010, pp. 319–350.

[54] TYC Tsai, RM Garner, and SG Megason. “Adhesion-based self-organization in tissue patterning”. In: *Annual Review of Cell and Developmental Biology* 38 (2022), pp. 349–374.

Supplementary Information to *Variations in nonlocal interaction range lead to emergent chase-and-run in heterogeneous populations*

K. J. Painter[1], V. Giunta[2], J. R. Potts[3], and S. Bernardi[4]

[1] *Dipartimento Interateneo di Scienze, Progetto e Politiche del Territorio (DIST), Politecnico di Torino, Viale Pier Andrea Mattioli 39, 10125, Turin, Italy*
[2] *Department of Mathematics, Swansea University, Computational Foundry, Bay Campus, Swansea SA1 8EN , UK*
[3] *School of Mathematics and Statistics, Hounsfield Road, University of Sheffield, UK, S3 7RH*
[4] *Department of Mathematical Sciences "G. L. Lagrange", Politecnico di Torino, Corso Duca degli Abruzzi 24, 10129 Torino, Italy*

A Individual based model

A.1 Model description

Here we describe the stochastic individual based model (IBM); as noted in the main text, the IBM is constructed in a manner that permits formal relation to the continuous model (Equations (1) in main manuscript) in an appropriate limit, demonstrated below. The IBM takes the form of a position jump random walk on a lattice, where we work on either a 1D line lattice of length L or a 2D square lattice of side L, with periodic boundary conditions. The lattice spacing is denoted l and defined so that L/l is an integer. We denote by $M(x,t)$ (resp. $N(x,t)$) the number of individuals from population C (resp. R) at lattice point x at time t. For the 1D model, we define

$$S^1_M(x,t) = \min\Bigg\{1, \max\Bigg\{-1, \phi\left(\frac{M(x)+N(x)}{l}\right)\left(\frac{\alpha_{CC}}{4r_{CC}}\sum_{y=-r_{CC}}^{r_{CC}} M(x+yl,t)\frac{y}{|y|} + \frac{\alpha_{CR}}{4r_{CR}}\sum_{y=-r_{CR}}^{r_{CR}} N(x+yl,t)\frac{y}{|y|}\right)\Bigg\}\Bigg\}, \tag{1}$$

$$S^1_N(x,t) = \min\Bigg\{1, \max\Bigg\{-1, \phi\left(\frac{M(x)+N(x)}{l}\right)\left(\frac{\alpha_{RR}}{4r_{RR}}\sum_{y=-r_{RR}}^{r_{RR}} N(x+yl,t)\frac{y}{|y|} + \frac{\alpha_{RC}}{4r_{RC}}\sum_{y=-r_{RC}}^{r_{RC}} M(x+yl,t)\frac{y}{|y|}\right)\Bigg\}\Bigg\}, \tag{2}$$

where $r_{CC}, r_{CR}, r_{RC}, r_{RR} < L/l$ are integers. In 2D, we define

$$S^2_{M1}(x,t) = \min\Bigg\{1, \max\Bigg\{-1, \phi\left(\frac{M(x)+N(x)}{l^2}\right)\left(\frac{\alpha_{CC}}{2\pi l r^2_{CC}}\sum_{\mathbf{y}\in B^2_{r_{CC}}} M(\mathbf{x}+\mathbf{y}l,t)\cos(\theta_{\mathbf{y}}) + \frac{\alpha_{CR}}{2\pi l r^2_{CR}}\sum_{\mathbf{y}\in B^2_{r_{CR}}} N(\mathbf{x}+\mathbf{y}l,t)\cos(\theta_{\mathbf{y}})\right)\Bigg\}\Bigg\}, \tag{3}$$

$$S^2_{M2}(x,t) = \min\Bigg\{1, \max\Bigg\{-1, \phi\left(\frac{M(x)+N(x)}{l^2}\right)\left(\frac{\alpha_{CC}}{2\pi l r^2_{CC}}\sum_{\mathbf{y}\in B^2_{r_{CC}}} M(\mathbf{x}+\mathbf{y}l,t)\sin(\theta_{\mathbf{y}}) + \frac{\alpha_{CR}}{2\pi l r^2_{CR}}\sum_{\mathbf{y}\in B^2_{r_{CR}}} N(\mathbf{x}+\mathbf{y}l,t)\sin(\theta_{\mathbf{y}})\right)\Bigg\}\Bigg\}, \tag{4}$$

where $\theta_{\mathbf{y}}$ is the direction of the vector $\mathbf{y}$. Functions $S^2_{N1}(x,t)$ and $S^2_{N2}(x,t)$ are defined analogously.

For the 1D random walk we assume that, in a time-step of length τ, there is some probability that an individual at x moves to one of the two adjacent lattice sites at $x \pm l$. For a member of population C, these probabilities are given by

$$p^1_{M\tau}(x \pm l|x) = \frac{1 \pm S^1_M(x,t)}{2}, \tag{5}$$

with an analogous expression for the probabilities of movement for members of population R.

In the 2D random walk, movements can take place to one of the four adjacent lattice sites, i.e. from position $\mathbf{x}$ to $\mathbf{x} \pm (l, 0)$ or $\mathbf{x} \pm (0, l)$. For a member of population C, these probabilities are given by

$$p^2_{M\tau}(\mathbf{x} \pm (l, 0)|\mathbf{x}) = \frac{1 \pm S^2_{M1}(\mathbf{x}, t)}{4}, \tag{6}$$

$$p^2_{M\tau}(\mathbf{x} \pm (0, l)|\mathbf{x}) = \frac{1 \pm S^2_{M2}(\mathbf{x}, t)}{4}, \tag{7}$$

with analogous expressions for the probabilities of movement for members of population R. To perform simulations, the IBMs were coded in C and the code can be found at `https://github.com/jonathan-potts/ChaseAndRun`.

A.2 From IBM to PDE

To relate the IBMs described in Equations (1)-(7) to the PDEs of Equations (1) in the main manuscript, we first take expectations and assume that covariances are negligible (i.e. a mean field approximation). With this assumption, the expected number of individuals, $M_E(x, t)$, from population C at lattice site x at time t obeys the following iterative equation in 1D

$$\begin{aligned} M_E(x, t + \tau) &= M_E(x - l, t)p^1_{C\tau}(x|x - l) + M_E(x + l, t)p^1_{C\tau}(x|x + l) \\ &= \frac{1}{2}[M_E(x - l, t)(1 + S^1_M(x - l, t)) + M_E(x + l, t)(1 - S^1_M(x + l, t))], \end{aligned} \tag{8}$$

and the equation for $N_E(x, t)$ (the expected number of individuals from population R at lattice site x at time t) is analogous. In 2D, the change in $M_E(x, t)$ over time is given by

$$\begin{aligned} M_E(\mathbf{x}, t + \tau) =& \frac{1}{4}[M_E(\mathbf{x} - (l, 0), t)(1 + S^2_{M1}(\mathbf{x} - (l, 0), t)) + M_E(\mathbf{x} + (l, 0), t)(1 - S^2_{M1}(\mathbf{x} + (l, 0), t)) \\ &+ M_E(\mathbf{x} - (0, l), t)(1 + S^2_{M2}(\mathbf{x} - (0, l), t)) + M_E(\mathbf{x} + (0, l), t)(1 - S^2_{M2}(\mathbf{x} + (0, l), t))]. \end{aligned} \tag{9}$$

For the 1D case, we rearrange Equation (8) to give

$$\begin{aligned} \frac{M_E(x, t + \tau) - M_E(x, t)}{\tau} = \frac{l^2}{2\tau}\Bigg[& \frac{M_E(x + l, t) - 2M_E(x, t) + M_E(x - l, t)}{l^2} \\ &- \frac{2}{l}\frac{S^1_M(x + l, t)M_E(x + l, t) - S^1_M(x - l, t)M_E(x - l, t)}{2l}\Bigg]. \end{aligned} \tag{10}$$

In 2D, a similar rearrangement gives

$$\begin{aligned} &\frac{M_E(\mathbf{x}, t + \tau) - M_E(\mathbf{x}, t)}{\tau} = \\ &\frac{l^2}{2\tau}\Bigg[\frac{M_E(\mathbf{x} + (l, 0), t) + M_E(\mathbf{x} + (0, l), t) - 4M_E(\mathbf{x}, t) + M_E(\mathbf{x} - (l, 0), t) + M_E(\mathbf{x} - (0, l), t)}{l^2} \\ &- \frac{2}{l}\frac{S^2_{M1}(\mathbf{x} + (l, 0), t)M_E(\mathbf{x} + (l, 0), t) - S^2_{M1}(\mathbf{x} - (l, 0), t)M_E(\mathbf{x} - (l, 0), t)}{2l} \\ &- \frac{2}{l}\frac{S^2_{M2}(\mathbf{x} + (0, l), t)M_E(\mathbf{x} + (0, l), t) - S^2_{M2}(\mathbf{x} - (0, l), t)M_E(\mathbf{x} - (0, l), t)}{2l}\Bigg]. \end{aligned} \tag{11}$$

We then take the limit as $l, \tau \to 0$ such that $d_n = l^2/(2n\tau)$ is kept constant (i.e. the diffusion limit). We also send $r_{ij} \to \infty$ keeping $\xi_{ij} = r_{ij}l$ constant, for each $i, j \in \{C, R\}$ and write $C(\mathbf{x}, t)$ (resp. $R(\mathbf{x}, t)$) for the limit of $M_E(\mathbf{x}_l, t)/l^n$ (resp. $N_E(\mathbf{x}_l, t)/l^n$) where $\mathbf{x}_l$ is the closest lattice site to the point $\mathbf{x}$ for any given l (using bold letters for both 1D and 2D here). A direct calculation of this limit leads to

$$\begin{aligned} \frac{\partial C}{\partial t} &= d_n\nabla \cdot \left[\nabla C - \frac{C\alpha_{CC}}{V_n(\xi_{CC})}\phi(C + R)\int_{\mathcal{B}^n_{\xi_{CC}}} C(\mathbf{x} + \mathbf{y}, t)e_{\mathbf{y}}\, d\mathbf{y} - \frac{C\alpha_{CR}}{V_n(\xi_{CR})}\phi(C + R)\int_{\mathcal{B}^n_{\xi_{CR}}} R(\mathbf{x} + \mathbf{y}, t)e_{\mathbf{y}}\, d\mathbf{y}\right], \\ \frac{\partial R}{\partial t} &= d_n\nabla \cdot \left[\nabla R - \frac{R\alpha_{RC}}{V_n(\xi_{RC})}\phi(C + R)\int_{\mathcal{B}^n_{\xi_{RC}}} C(\mathbf{x} + \mathbf{y}, t)e_{\mathbf{y}}\, d\mathbf{y} - \frac{R\alpha_{RR}}{V_n(\xi_{RR})}\phi(C + R)\int_{\mathcal{B}^n_{\xi_{RR}}} R(\mathbf{x} + \mathbf{y}, t)e_{\mathbf{y}}\, d\mathbf{y}\right]. \end{aligned} \tag{12}$$

In the case $d_n = 1$, this is the same as Equations (1) in the main manuscript for $D_C = D_R = 1$. The case $D_C = D_R = d_n = 1$ is the only case we are interested in for our numerical analysis. However, note that one could set $d \neq 0$ and rescale the $\alpha'_{ij}s$ to return Equations (1) of the manin manuscript for any non-zero values of D_C and D_R, if required. We leave this general case as an exercise for any interested reader.

Finally, when comparing between IBM and PDE formulation, it is possible rescale by any constant A, by setting $C \mapsto C/A$, $R \mapsto R/A$, and $\alpha_{ij} \mapsto A\alpha_{ij}$, for $i, j \in \{C, R\}$. This can be valuable, as the total mass in the IBM version is by definition the number of individuals. Therefore this rescaling allows comparisons can be made between a single set of PDEs, where the total mass of A and B is fixed across all the PDE analysis, and corresponding IBMs with different numbers of individuals.

B Linear Stability Analysis

Following the standard approach (e.g. [1]), we consider small heterogeneous perturbations of the spatially uniform steady state (C_s, R_s), i.e. $C(\mathbf{x}, t) = C_s + \tilde{C}(\mathbf{x}, t)$ and $R(\mathbf{x}, t) = R_s + \tilde{R}(\mathbf{x}, t)$, with $|\tilde{C}(\mathbf{x}, t)|, |\tilde{R}(\mathbf{x}, t)| \ll 1$. Substituting into Equations (1) of the main manuscript, linearising about (C_s, R_s), and looking for solutions of the form $\tilde{C}, \tilde{R} \propto e^{i\mathbf{k}\cdot\mathbf{x}+\lambda t}$ (where $\mathbf{k}$ denotes the wave-vector and λ is the growth rate) leads to the dispersion relation

$$\lambda^2 + \mathcal{C}(k)\lambda + \mathcal{D}(k) = 0, \tag{13}$$

where $\mathcal{C}(k)$ and $\mathcal{D}(k)$ are given by

$$\mathcal{C}(k) = k^2(D_C + D_R) - k\,(\Lambda_{CC} + \Lambda_{RR}) \tag{14a}$$

$$\mathcal{D}(k) = D_C\,D_R\,k^4 - k^3\,(D_R\,\Lambda_{CC} + D_C\,\Lambda_{RR}) + k^2\,(\Lambda_{CC}\,\Lambda_{RR} - \Lambda_{CR}\Lambda_{RC})\,. \tag{14b}$$

Each Λ_{uv} function represents the nonlocal contribution for each interaction and is evaluated as proposed in [2], where the authors extend pattern formation analysis to higher spatial dimension for models of form (1a)-(1b). They are given by:

$$\Lambda_{UV} = U_s\,\frac{2\pi^{\frac{n}{2}}}{\Gamma(\frac{n}{2})}\,\frac{\alpha_{UV}}{V_n(\xi_{UV})}\,\phi(U_s + V_s)\int_0^{\xi_{UV}} y^{n-1}\,j_1^{(n)}(ky)\,dy, \tag{15}$$

where $k = |\mathbf{k}|$, $y = |\mathbf{y}|$ and $U, V \in \{C, R\}$ with corresponding homogeneous steady state $U_s, V_s \in \{C_s, R_s\}$. In the expression above, $j_1^{(n)}(\mathbf{x})$ denote the first order n^{th} dimensional hyperspherical Bessel functions. In particular, $j_1^{(1)}(x) = \sin(x)$ and $j_1^{(2)}(x) = J_1(kx)$, where J_1 denotes the first order Bessel function of the first kind.

In 1D ($n = 1$), after a few rearrangements, the nonlocal terms in Eq. (15) reduce to

$$\Lambda_{UV} = U_s\alpha_{UV}\phi(U + V)\Gamma_{UV}, \quad \text{where } \Gamma_{UV} = \frac{1 - \cos(\xi_{UV}\,k)}{\xi_{UV}\,k}, \tag{16}$$

for $U, V \in \{C, R\}$, $U_s \in \{C_s, R_s\}$.

In 2D ($n = 2$), we instead have

$$\Lambda_{UV} = 2U_s\frac{\alpha_{UV}}{\xi_{UV}^2}\phi(U_s + V_s)\left(-\frac{\xi_{UV}}{k}J_0(k\xi_{UV}) + \frac{1}{k^2}\int_0^{k\xi_{UV}} J_0(p)dp\right), \tag{17}$$

where J_0 is the zero order Bessel function of the first kind.

To assess the potential for pattern formation, we investigate when the uniform steady state is stable to spatially homogeneous perturbations (i.e. $\Re(\lambda^+(0)) \leq 0$, where $\lambda^+ = 0.5(-\mathcal{C} + \sqrt{\mathcal{C}^2 - 4\mathcal{D}})$) and unstable to spatially inhomogeneous perturbations (i.e. $\Re(\lambda^+(k)) > 0$, for some $k > 0$ – we refer to any such k as unstable wavenumbers). The former condition is always satisfied. The latter holds if and only if $\mathcal{C}(k) < 0$ or $\mathcal{D}(k) < 0$, for some positive k. The tractability of the 1D dispersion relation allows for the derivation of some general insights. Specifically, in 1D (using the simplified form $\phi \equiv 1$ for consistency with our numerics) the condition on $\mathcal{C}$ gives

$$C_s\,\alpha_{CC}\,\xi_{CC} + R_s\,\alpha_{RR}\,\xi_{RR} > 2\,(D_C + D_R), \tag{18}$$

which shows that an instability is possible when the positive homotypic interactions dominate over diffusion: i.e. at least one of the populations has a sufficiently strong self-attraction.

Moreover, for instances in which pattern formation is predicted, we distinguish between *Turing instabilities* (i.e. $\Im(\lambda^+(k)) = 0$ for unstable wavenumbers) and *Turing-wave instabilities* (when $\Im(\lambda^+(k)) \neq 0$ for at least one of the unstable wavenumbers); in the latter, solutions are expected to oscillate in space and time as they diverge from the uniform steady state. Turing-wave patterns require $\mathcal{C}^2(k) - 4\mathcal{D}(k) < 0$ and, for the 1D model with $\phi \equiv 1$ and $D_C = D_R = 1$, this leads to

$$(C_s\,\alpha_{CC}\,\xi_{AA} - R_s\,\alpha_{RR}\,\xi_{RR})^2 + 4C_s\,R_s\,\alpha_{CR}\,\xi_{CR}\,\alpha_{RC}\,\xi_{RC} < 0, \tag{19}$$

Thus, in 1D, Turing-wave patterns may be possible under a sufficiently strong chase-and-run interaction to emerge.

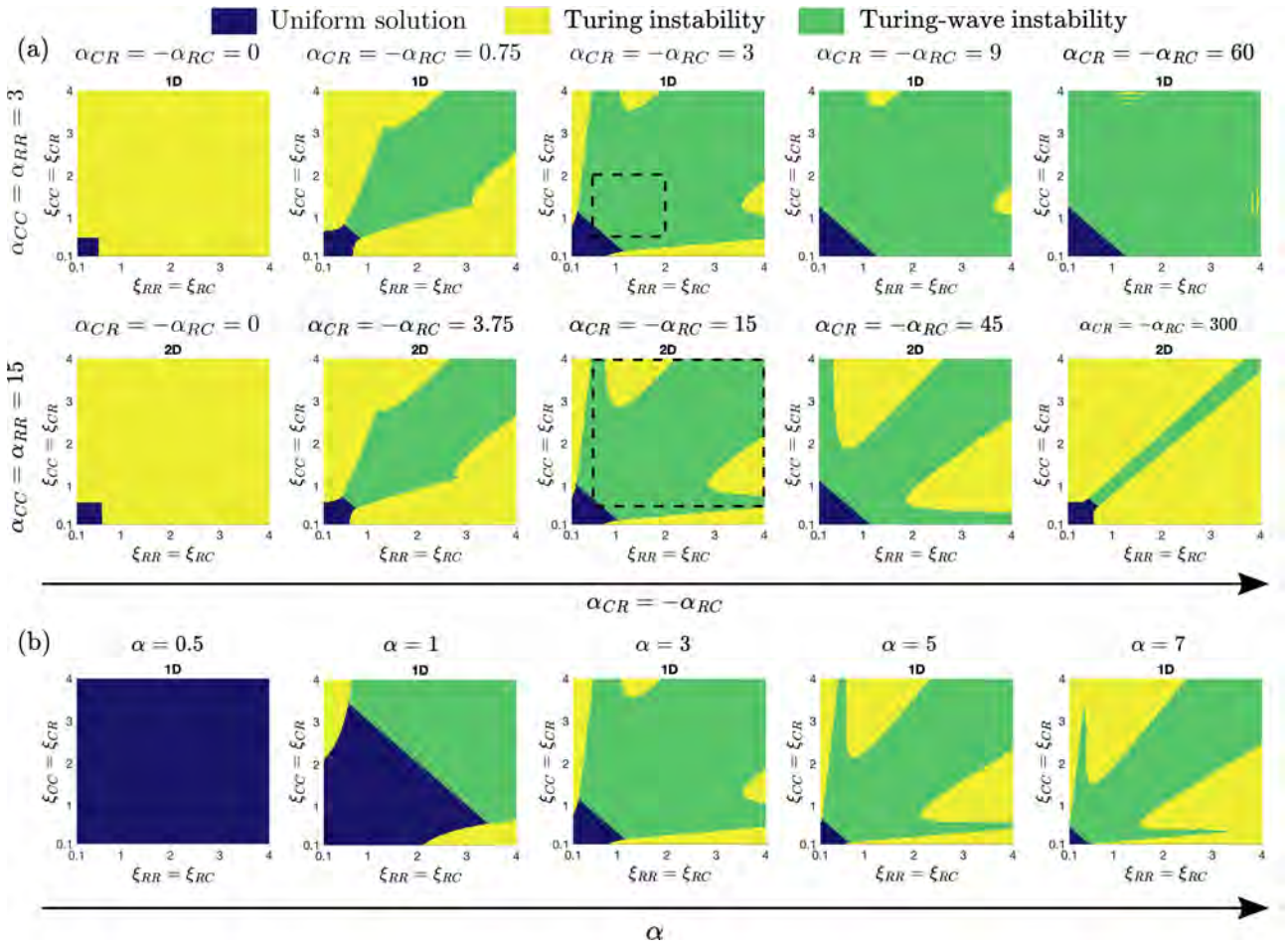

Figure S1: Parameter spaces for pattern formation predicted by the LSA in 1D and 2D, for increasing values of (a) the chase-and-run interactions and (b) all interactions ranges. We classify the resulting solutions as: uniform solution (blue), stationary pattern (yellow), dynamic pattern (green). The dotted boxes highlight the values considered in the numerical studies presented in the main text, compare respectively with Figure 3(a) (1D) and Figure 4(a) (2D). We adopt $\phi(C,R) = 1$ in 1D, $\phi(C,R) = 1/(1+C+R)$ in 2D. Other model parameters are set as $D_C = D_R = 1$, $C_s = R_s = 1$.

In Figure S1 we plot the predicted parameter space for patterning in both 1D (using $\phi \equiv 1$) and 2D (using $\phi \equiv 1/(1+C+R)$) across (ξ_R, ξ_C) space. Note that the middle panels in Figure S1(a) in the top and bottom rows correspond to the simulation study settings of Figure 3(a) and Figure 4(a), respectively. In both instances, the regions of predicted patterning match with the results of the numerical simulations. Moreover, the growth rate – by which we mean $\max\{\Re(\lambda^+(k))\}$, an indicator of how quickly solutions are expected to diverge from the steady state – is found to increase if we move away from the stability region (paths (i)-(ii)-(iii), (i)-(ii)-(iii)-(iv), (i)-(ii)-(iii)-(v)) of Figure 3(a), see also Figure S2(a). From left to right we show the impact of an increasingly strong chase-and-run interaction which, for a moderate interaction leads to a broad transition from Turing to Turing-wave type instabilities. A more dominant chase-and-run, though, has a diverging impact in 1D and 2D, where in the former we observe that in 1D patterns are near ubiquitously predicted to be of Turing-wave like, while in 2D they are of Turing-like. This is consistent with the significant differences between 1D and 2D noted previously in [2]. We note that if we simultaneously increase all interaction strengths, any regions of uniform solutions are found to reduce and instabilities are predicted to form under smaller interaction ranges, see Figure S1(b).

Finally, under a strong chase-and-run parameter setting and in the absence of homotypic interactions ($\alpha_{CC} = \alpha_{RR} = 0$), the sign structure in the Jacobian matrix reveals that when $\xi_C > \xi_R$ the two populations exhibit an out-of-phase Turing instability (the entries in the rows of the Jacobian matrix have the same sign). Otherwise, the two populations remain in-phase in the emerging pattern (the entries in the rows of the Jacobian matrix have opposite sign), see Figure S2(b). This further reinforces the potentially strong influence of interaction range on the system.

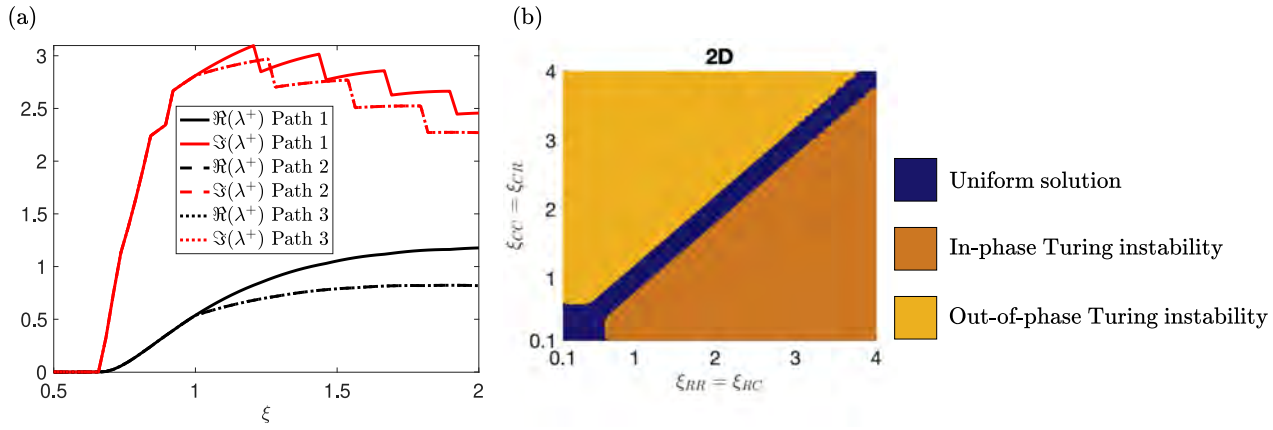

Figure S2: (a) Real and imaginary parts of λ^+ for different values of the sensing range ξ. In particular, Path 1 corresponds to the diagonal of Figure 3(a); Path 2 corresponds to path (i)-(ii)-(iii)-(iv) of Figure 3(a); Path 3 corresponds to path (i)-(ii)-(iii)-(v) of Figure 3(a). (b) Parameter space for pattern formation predicted by the LSA in 2D, for $\alpha_{CC} = \alpha_{RR} = 0$, $\alpha_{CR} = -\alpha_{RC} = 300$. We classify the resulting solutions as: uniform solution (blue), in-phase Turing instability (brown), out-of-phase Turing instability (orange). We adopt $\phi(C, R) = 1/(1 + C + R)$. Other model parameters are set as $D_C = D_R = 1$, $C_s = R_s = 1$.

C Numerical methods

For the 1D simulations we adopt a Method of Lines approach. Specifically, we discretise the domain $[0, L]$ into a regular lattice of spacing Δx and solve the resultant system of time-dependent ODEs. Note that the discretisation of the nonlocal terms exploits a Fast Fourier Transform technique to efficiently calculate the integral: full details of the numerical method itself are provided in [3]. For all 1D simulations we have set $\Delta x = 0.05$. The code used to solve Equations (1) of the main manuscript in 1D is available at `https://zenodo.org/records/13772853`. For the 2D simulations we use the spectral numerical scheme described in [4]. We discretise the spatial domain $[0, L] \times [0, L]$ by defining the grid points (x_i, y_j), where $x_i = i\Delta x$, $y_j = j\Delta y$, and $i, j \in \{0, 1, \ldots, 2^n - 1\}$, with $n = 7$ for $L = 10$, and $n = 8$ for $L = 20$. The code used to solve Equations (1) of the main manuscript in 2D is available at at `https://zenodo.org/records/13772853`.

D Additional figures

References

[1] JD Murray. *Mathematical biology II: spatial models and biomedical applications*. Vol. 18. Springer, 2003.

[2] TJ Jewell, AL Krause, PK Maini, and EA Gaffney. "Patterning of nonlocal transport models in biology: the impact of spatial dimension". In: *Mathematical Biosciences* 366 (2023), p. 109093.

[3] A Gerisch. "On the approximation and efficient evaluation of integral terms in PDE models of cell adhesion". In: *IMA journal of numerical analysis* 30.1 (2010), pp. 173–194.

[4] V Giunta, T Hillen, M Lewis, and JR Potts. "Local and global existence for nonlocal multispecies advection-diffusion models". In: *SIAM Journal on Applied Dynamical Systems* 21.3 (2022), pp. 1686–1708.

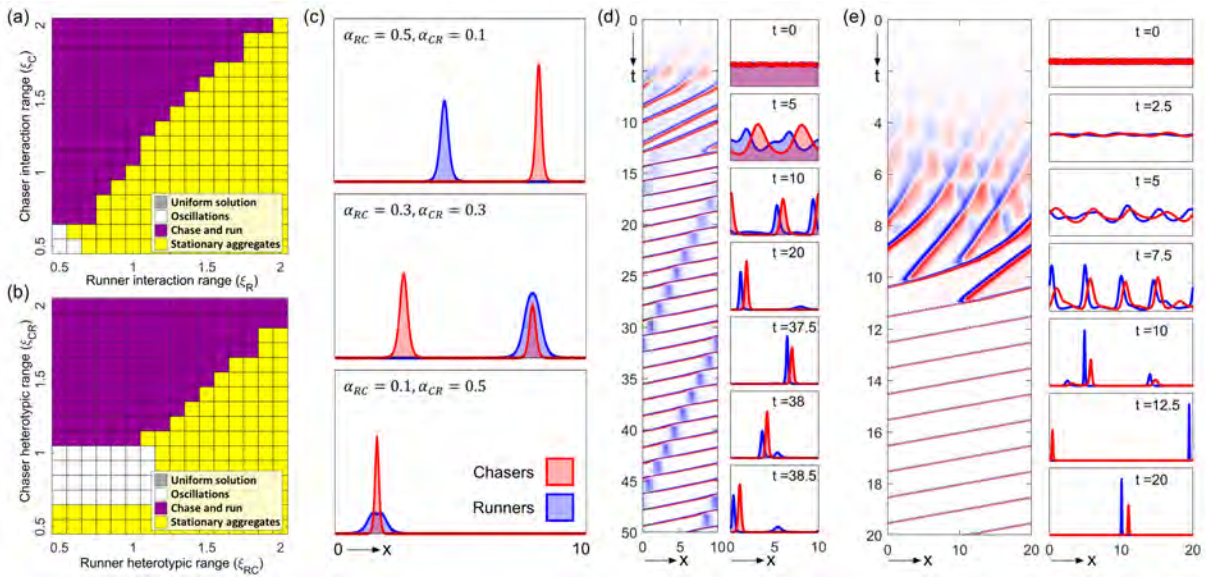

Figure S3: (a) Pattern selection across interaction range space. The form of pattern is classified following a simulation at each (ξ_C, ξ_R) pair as: uniform solution (gray), spatiotemporal oscillations (white), population chase-and-run (magenta), stationary aggregates (yellow). Here, $\alpha_{CC} = \alpha_{CR} = -\alpha_{RC} = \alpha_{RR} = 5$. (b) Pattern selection across heterotypic interaction range space (ξ_{RC}, ξ_{CR}). We set $\xi_{CC} = \xi_{RR} = 1$ and $\alpha_{CC} = \alpha_{CR} = -\alpha_{RC} = \alpha_{RR} = 3$. (c) Different forms of stationary aggregate when $1 = \xi_C < \xi_R = 1.5$ and $\alpha_{CC} = \alpha_{RR} = 3$: (top) completely segregated, $\alpha_{CR} = 1$ $\alpha_{RC} = -5$; (middle) mixed/segregated, $\alpha_{CR} = 3$ $\alpha_{RC} = -3$; (bottom) completely mixed, $\alpha_{CR} = 5$ $\alpha_{RC} = -1$. (d) Chase-and-run, where a group of runners is periodically dropped. $\xi_C = 1.5$, $\xi_R = 1$, $\alpha_{CC} = \alpha_{CR}, \alpha_{RR} = 3$, $\alpha_{RC} = -1.5$. (e) Chase-and-run on a larger domain $\xi_C = 1.5, \xi_R = 1$, $\alpha_{CC} = \alpha_{CR} = \alpha_{RR} = 3, \alpha_{RC} = -3$. For all simulations in this figure, $D_C = D_R = R_S = C_S = 1$ and initial conditions are dispersed on a domain of length $L = 10$ for panels (a) - (d), and $L = 20$ for panel (e).

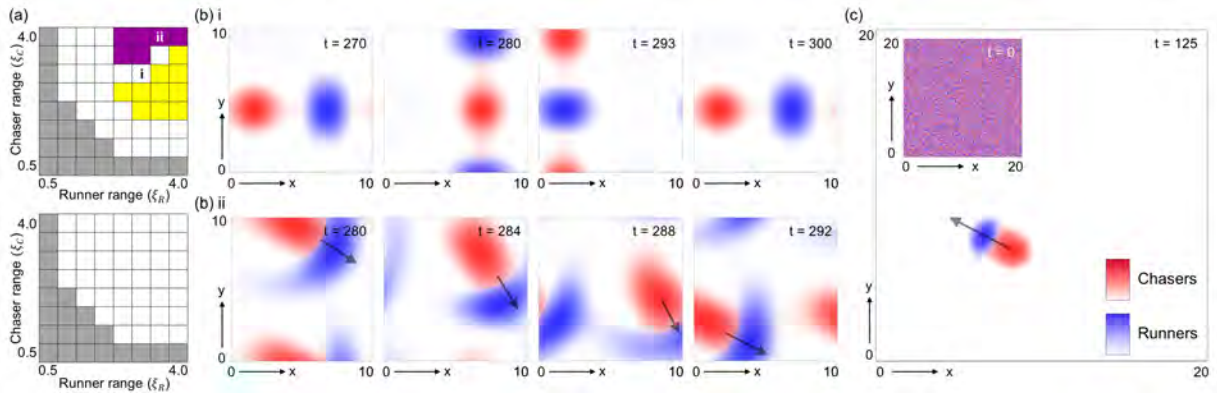

Figure S4: (a) Pattern selection across (ξ_R, ξ_C) space for 2D simulations. The form of pattern is classified following a simulation at each (ξ_R, ξ_C) pair as: uniform solution (gray), spatiotemporal oscillations (white), population chase-and-run (magenta), stationary aggregates (yellow). For the top panel we consider uniformly weak interaction strengths ($\alpha_{CC} = \alpha_{CR} = -\alpha_{RC} = \alpha_{RR} = 6$), while for the bottom panel homotypic interaction strengths are weak ($\alpha_{CC} = \alpha_{RR} = 6$) but heterotypic interaction strengths are strong ($\alpha_{CR} = -\alpha_{RC} = 20$). (b) Snapshots for the simulations marked in (a, top panel), showing (i) periodic oscillations; (ii) chase-and-run. (c) Simulation of the 2D model on a larger domain, showing that chase-and-run still forms robustly – the configuration shown at $t = 125$ persistently moves in the direction of the arrow with constant shape and speed. Note that the interaction strength and ranges for this simulation are as in Figure 4. For all simulations in this figure $D_C = D_R = R_s = C_s = 1$ and initial conditions are dispersed.